



Dynamics of greenhouse gases (CO₂, CH₄, N₂O) along the Zambezi River and major tributaries, and their importance in the riverine carbon budget

C. R. Teodoru¹, F. C. Nyoni², A. V. Borges³, F. Darchambeau³, I. Nyambe², and S. Bouillon¹

¹KU Leuven, Department of Earth and Environmental Sciences, Leuven, Belgium

²University of Zambia, Integrated Water Research Management Centre, Lusaka, Zambia

³University of Liège, Chemical Oceanography Unit, Liège, Belgium

Correspondence to: C. R. Teodoru (teo.teodoru@ees.kuleuven.be)

Received: 22 October 2014 – Published in Biogeosciences Discuss.: 27 November 2014

Revised: 12 March 2015 – Accepted: 2 April 2015 – Published: 24 April 2015

Abstract. Spanning over 3000 km in length and with a catchment of approximately 1.4 million km², the Zambezi River is the fourth largest river in Africa and the largest flowing into the Indian Ocean from the African continent. We present data on greenhouse gas (GHG: carbon dioxide (CO₂), methane (CH₄), and nitrous oxide (N₂O)) concentrations and fluxes, as well as data that allow for characterization of sources and dynamics of carbon pools collected along the Zambezi River, reservoirs and several of its tributaries during 2012 and 2013 and over two climatic seasons (dry and wet) to constrain the interannual variability, seasonality and spatial heterogeneity along the aquatic continuum. All GHG concentrations showed high spatial variability (coefficient of variation: 1.01 for CO₂, 2.65 for CH₄ and 0.21 for N₂O). Overall, there was no unidirectional pattern along the river stretch (i.e., decrease or increase towards the ocean), as the spatial heterogeneity of GHGs appeared to be determined mainly by the connectivity with floodplains and wetlands as well as the presence of man-made structures (reservoirs) and natural barriers (waterfalls, rapids). Highest CO₂ and CH₄ concentrations in the main channel were found downstream of extensive floodplains/wetlands. Undersaturated CO₂ conditions, in contrast, were characteristic of the surface waters of the two large reservoirs along the Zambezi mainstem. N₂O concentrations showed the opposite pattern, being lowest downstream of the floodplains and highest in reservoirs. Among tributaries, highest concentrations of both CO₂ and CH₄ were measured in the Shire River, whereas low values were characteristic of more turbid systems such as the Lu-

angwa and Mazoe rivers. The interannual variability in the Zambezi River was relatively large for both CO₂ and CH₄, and significantly higher concentrations (up to 2-fold) were measured during wet seasons compared to the dry season. Interannual variability of N₂O was less pronounced, but higher values were generally found during the dry season. Overall, both concentrations and fluxes of CO₂ and CH₄ were well below the median/average values for tropical rivers, streams and reservoirs reported previously in the literature and used for global extrapolations. A first-order mass balance suggests that carbon (C) transport to the ocean represents the major component (59 %) of the budget (largely in the form of dissolved inorganic carbon, DIC), while 38 % of the total C yield is annually emitted into the atmosphere, mostly as CO₂ (98 %), and 3 % is removed by sedimentation in reservoirs.

1 Introduction

Contrary to the earlier perception of inland waters as simple pipelines passively transporting significant amounts of both organic and inorganic carbon (C) to the ocean, it is increasingly recognized that freshwater ecosystems are capable of processing large quantities of C derived from the surrounding landscape, being therefore active components of global C cycling. Global figures based on recent data compilations suggest that the amount of C processed and emitted into the atmosphere from inland waters offsets the overall C transport to the global ocean (Cole et al., 2007; Tranvik et al., 2009;

Aufdenkampe et al., 2011; Bastviken et al., 2011; Butman and Raymond, 2011; Raymond et al., 2013). This amount of terrestrial C processed in rivers, lakes and reservoirs reaches approximately half the magnitude of the oceanic CO₂ sink (IPCC, 2013), a value that is similar to or even higher in magnitude than C uptake by terrestrial ecosystem (Aufdenkampe et al., 2011; IPCC, 2013). Despite large uncertainties related to these global estimates, it has become evident that freshwater ecosystems play a vital role in C budgets, disproportional to their areal extent (Cole et al., 2007). Quantifying the role of freshwater ecosystems as C sources and sinks and understanding the link between terrestrial and aquatic ecosystem as well as the underlying biogeochemical processes are therefore fundamental for quantitative estimates of the impact of land-use-related changes in C dynamics and for improving estimates of ecosystem C budgets.

Although rivers represent key elements of freshwater ecosystems, their role in global or regional C budgets is still unclear. Resulting from groundwater inputs of dissolved inorganic C (DIC) and from the mineralization of terrestrial organic C (OC; Battin et al., 2009), supersaturation in CO₂ has been reported for large rivers in boreal, temperate and tropical areas (Cole and Caraco, 2001; Richey et al., 2002; Aufdenkampe et al., 2011; Raymond et al., 2013; Bouillon et al., 2014; Abril et al., 2014, 2015). Studies of CO₂ dynamics in low-order rivers in temperate and boreal regions have also shown that these systems are extremely dynamic in terms of DIC (Guasch et al., 1998; Worrall et al., 2005; Waldron et al., 2007) and generally highly supersaturated in CO₂ (Kling et al., 1991; Hope et al., 2001; Finlay, 2003; Teodoru et al., 2009). Controlled by several biogeochemical processes (i.e., organic matter oxidation, photosynthesis and respiration, and exchange with atmosphere) and characterized by distinct isotopic signature, DIC stable isotopes ($\delta^{13}\text{C}$ -DIC) represent a powerful tool which can be used to distinguish between different riverine DIC sources (i.e., atmospheric/soil CO₂ or carbonate dissolution), to trace the DIC transport to the ocean and to assess the carbon transformation in the river itself. Data on tropical rivers and streams are particularly scarce compared to other regions, despite their high contribution (more than half) to the global freshwater discharge to the ocean and their particularly high importance in terms of riverine transport of sediments and C (Ludwig et al., 1996; Schlünz and Schneider, 2000) and the suggested higher areal CO₂ outgassing rates than temperate or boreal rivers (Aufdenkampe et al., 2011). While our understanding of C dynamics in tropical regions comes mostly from studies of the Amazon River basin, to date only a handful of studies explored the biogeochemical functioning of equally important African rivers such as the Bia, Comoé and Tanoé rivers in Côte d'Ivoire (Koné et al., 2009, 2010); the Tana (Kenya) and the Oubangui rivers (Congo River basin; Bouillon et al., 2009, 2012, 2014; Tamooh et al., 2012, 2013); the Congo River (Wang et al., 2013; Mann et al., 2014); and the Athi–Galana–Sabaki River (Kenya; Marwick et al., 2014).

Constraining the overall importance of rivers in the global C budget therefore requires an improved understanding of C cycling in other tropical and subtropical regions.

As part of a broader study on catchment-scale biogeochemistry of African rivers, the present study examines the spatiotemporal dynamics of CO₂, CH₄ and N₂O concentrations and fluxes in the Zambezi River basin based on three sampling campaigns extended over two climatic seasons (wet 2012, wet 2013 and dry 2013). The study quantifies the magnitude of CO₂ and CH₄ concentrations and fluxes, identifies the main C sources and the controlling factors responsible for the observed patterns, and examines hotspots for GHG exchange with the atmosphere. Finally, we make a first attempt at a C mass balance for the Zambezi River over the study period by budgeting emissions, sinks and transport of C.

2 Materials and methods

2.1 The Zambezi River – general characteristics

The Zambezi River is the fourth largest river in Africa in terms of discharge after the Congo, Nile and Niger, and the largest flowing into the Indian Ocean from the African continent. The river originates in northwest Zambia (11.370° S, 024.308° E; 1450 m a.s.l.) and flows southeast over 3000 km before it discharges into the Indian Ocean in Mozambique (Fig. 1). Based on distinct geomorphological characteristics, the Zambezi River is divided into three major segments: (i) the upper Zambezi from the headwaters to Victoria Falls; (ii) the middle Zambezi, from Victoria Falls to the edge of the Mozambique coastal plain (below Cahora Bassa Gorge); and (iii) the lower Zambezi, the stretch traversing the coastal plain down to the Indian Ocean (Wellington, 1955; Moore et al., 2007). The upper reaches of the river are incised into upper Precambrian crystalline basement rocks composed of metamorphosed sediments including shale, dolomite and quartzite. Further downstream, the Zambezi widens into the Barotse Floodplain, a very low gradient stretch that traverses unconsolidated sands, known as the Kalahari Sand. Downstream of the Barotse Floodplain, the gradient of the Zambezi steepens and the river begins to incise into Karoo-age basalts and sediments (sandstone, shale, limestone) that form the sub-Kalahari bedrock, creating a series of rapids and falls with Victoria Falls (world's second largest: 1708 m width, 108 m height) marking the edge of the upper Zambezi stretch (Moor et al., 2007). The middle Zambezi is characterized by a markedly steeper gradient than the section above the falls with an initial turbulent course through a series of narrow zigzag gorges and rapids before the river widens into the broad basins of the Kariba and Cahora Bassa reservoirs. Karoo-age basalts and sediments and subordinate Precambrian crystalline basement rocks (gneiss and granite) constitute the bedrock over most of this stretch of the river (Moore

et al., 2007). Downstream of the Cahora Bassa Reservoir, the river flows through one last gorge (the Cahora Bassa Gorge) before entering a more calm and broader stretch of the lower Zambezi. Traversing the Cretaceous and Tertiary sedimentary cover of the Mozambique coastal plain, the lower reaches of the river forms a large, 100 km long floodplain–delta system of oxbows, swamps and multichannel meanders.

Along its course, the Zambezi River collects water from many tributaries from both left and right banks (Fig. 1) which contribute to different extents to the annual average discharge, which ranges between 3424 and 4134 m³ s⁻¹ (Beilfuss and dos Santos, 2001; World Bank, 2010). With a mean discharge of 320 m³ s⁻¹, the Kafue River is the major tributary of the Zambezi. The river originates in northwest Zambia, flows south-southeast for over 1550 km and joins the Zambezi River ~70 km downstream of the Kariba Dam. Its drainage basin of over 156 000 km², which lies entirely within Zambia, is home to almost half of the country's population, and has a large concentration of mining, industrial and agricultural activities.

There are two major impoundments along the Zambezi River. The Kariba Reservoir, completed in 1959 between Zambia and Zimbabwe, about 170 km downstream of Victoria Falls (Fig. 1), is the world's largest reservoir by volume (volume: 157 km³; area: 5364 km²; Kunz et al., 2011a). Completed in 1974 in Mozambique, about 300 km downstream of the Kariba Dam (Fig. 1), the Cahora Bassa Reservoir is the fourth largest reservoir in Africa (volume: 52 km³; area: 2675 km²; Beilfuss and dos Santos, 2001). Contemporaneous with the construction of the Cahora Bassa Dam, two smaller reservoirs have been created on the Kafue River: (i) the Kafue Gorge Reservoir (volume: ~1 km³; area: 13 km²) completed in 1972 about 75 km upstream from the confluence with the Zambezi with the purpose of power generation, and (ii) the Itezhi Tezhi Reservoir (volume: ~6 km³; area: 365 km²) completed in 1978 about 270 km upstream (Fig. 1), which serves as a storage reservoir to ensure constant water supply for the Kafue Gorge Dam.

The climate of the Zambezi Basin, classified as humid subtropical, is generally characterized by two main seasons: the rainy season from October/November to April/May, and the dry season from May/June to September/October (Fig. 2). Annual rainfall across the river basin (mean 940 mm for the entire catchment) varies with latitude from about 400 to 500 mm in the extreme south and southwest part of the basin to more than 1400 mm in the northern part and around Lake Malawi (Chenje, 2000). Up to 95 % of the annual rainfall in the basin occurs during the rainy season, while irregular and sporadic rainfall events during the dry period contribute generally up to 5 %. Driven by seasonality in rainfall patterns, the hydrological cycle of the Zambezi River has a bimodal distribution, characterized by a single main peak flood with maximum discharge occurring typically in April/May and minimum in November. An example of the seasonality and the

disturbance of the natural flow pattern associated with river damming is illustrated in Fig. 2, based on daily discharge data measured at four sites in the basin between January 2012 and January 2014.

Almost 75 % of the basin is covered by forest and bush. Cropped land (with mostly rain-fed agriculture) covers up to 13 %, and grassland cover about 8 % of the land area (SADC et al., 2012). Wetlands, comprising swamps, marshes and seasonally inundated floodplains, cover more than 5 % of the total basin area (SADC et al., 2012; McCartney et al., 2013). Important wetlands in the basin include the Lungue Bungo Swamps, Luena Flats, Barotse Floodplain, Kafue Flats and Luangwa Floodplain in Zambia; the Mid-Zambezi Valley and Mano Pools in Zimbabwe; the Shire Marshes in Malawi; and the lower Zambezi and Zambezi Delta in Mozambique (McCartney et al., 2013).

In 1998, the population in the basin was estimated to be 31.7 million (one-third of the total population of the eight basin countries), out of which more than 85 % live in Malawi, Zambia and Zimbabwe. Ten years later (2008) the population reached over 40 million, and it is predicted to reach 51.2 million by 2025 (SADC et al., 2012). This predicted increase in population, alongside ongoing economical development in the region and new hydropower projects, is expected to exert further pressure on the aquatic environment and natural water resources of the basin.

2.2 Sampling strategy and analytical techniques

Sampling was conducted during two consecutive years and over two climatic seasons: wet season (1 February to 5 May) 2012, wet season (6 January to 21 March) 2013, and dry season (15 October to 28 November) 2013 (Fig. 2). Up to 56 sites were visited during each campaign, depending on logistics and accessibility. Sampling sites (chosen at 100–150 km apart) were located as follows: 26 along the Zambezi main-stream (including 3 sites on the Kariba and 3 on the Cahora Bassa reservoirs), 2 on the Kabompo, 13 along the Kafue (including 3 on the Itezhi Tezhi Reservoir), 3 on the Lunga (main tributary of the Kafue), 5 along the Luangwa, 2 on the Lunsemfwa (main tributary of the Luangwa), 1 on the Mazoe and 1 on the Shire River (Fig. 1). In situ measurements and water sampling was performed, whenever possible, from boats or dugout canoes in the middle of the river at ~0.5 m below the water surface. However, in the absence of boats/canoes, sampling was carried out either from bridges or directly from the shore and as far as possible away from the shoreline.

At each location, in situ measurements of water temperature, dissolved oxygen (DO), conductivity and pH were performed with a YSI ProPlus multimeter probe. The pH and DO probes were calibrated each time before the measurement using United States National Bureau of Standards buffer solutions of 4 and 7 and water-saturated air. The partial pressure of CO₂ (*p*CO₂) in the water was measured

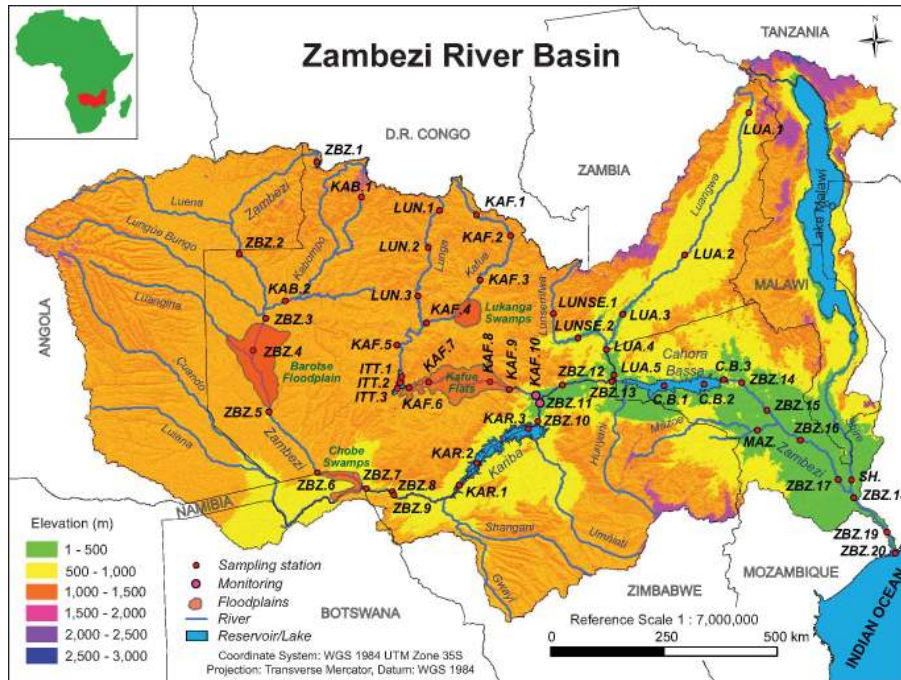


Figure 1. Map of the Zambezi River basin illustrating the location within Africa, the shared area of the basin within the eight African nations, the elevation gradient, the main hydrological network and the distribution of sampling sites along the Zambezi mainstem and major tributaries.

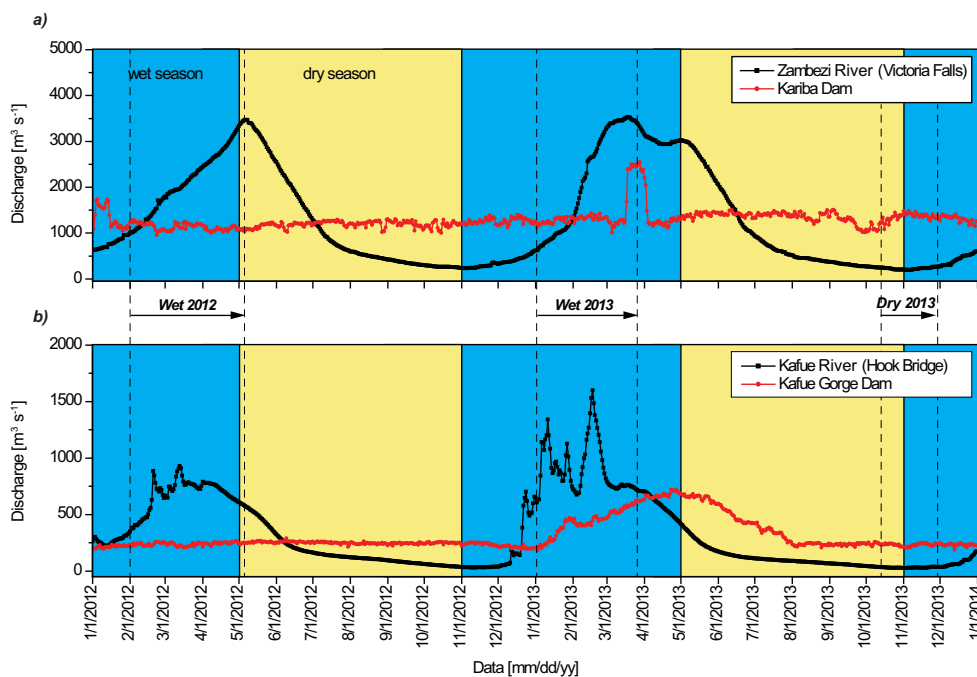


Figure 2. Water discharge for (a) the Zambezi River at Victoria Falls power station and the disturbance of natural flow pattern by dam operation at Kariba Dam, and (b) for the Kafue River at Hook Bridge (upstream of the Itezhi Tezhi Reservoir) and the regulated flow at the Kafue Gorge Dam between January 2012 and January 2014 (data from Zambia Electricity Supply Corporation Limited, ZESCO).

in situ with a PP Systems EGM-4 non-dispersive, infrared gas analyzer (calibrated before each trip with a certified gas standard with a mixing ratio of 1017 ppm) using both a Liqui-Cel MiniModule membrane contactor equilibrator and a headspace technique. For the first method, the water pumped from ~ 0.5 m depth was circulated through the exchanger at a constant flow rate of ~ 0.35 L min $^{-1}$, and the gases were continuously re-circulated in a closed loop into the EGM-4 for instantaneous measurements of $p\text{CO}_2$. At a flow rate of 0.35 L min $^{-1}$, the half-equilibration time of CO_2 in the MiniModule is 4–5 s. For the headspace technique, 30 mL of water, collected (under the water) into five 60 mL polypropylene syringes, was mixed with 30 mL of air of known CO_2 concentration and gently shaken for 5 min to allow for equilibration of the two phases. The headspace volume (30 mL) was then transferred into a new syringe and directly injected into the EGM-4 analyzer. Water $p\text{CO}_2$ was calculated from the ratio between the air and water volumes using the gas solubility at sampling temperature. Comparison between the syringe-headspace and membrane equilibrator techniques gave consistent results, with a slope not significantly different from unity (1.09), $r^2 = 0.992$, $p < 0.0001$, $n = 83$, in the 140–14 000 ppm range (Abril et al., 2015).

CO_2 fluxes to the atmosphere were measured using a custom-designed floating chamber (polyvinyl chloride cylinder of 38 cm internal diameter, 15 cm active height, plus 7 cm skirt under the air–water interface) connected at the top through two rubber-polymer tubes ($\varnothing = 0.45$ cm) to a non-dispersive infrared analyzer (PP Systems, EGM-4). Starting at atmospheric concentration (and pressure), the air inside the chamber (17 L volume) was circulated in a closed loop and analyzed for CO_2 with readings every 30 s over a 30 min period. Temperature inside the chamber was monitored continuously with a VWR 4039 waterproof thermometer (accuracy ± 1 °C) and further used in the flux calculation. For the determination of CH_4 fluxes, a 60 mL syringe, fitted on a third tube with a two-way valve, was filled with 30 mL of air from inside the chamber at 0, 5, 10, 20 and 30 min intervals. Transferred immediately into a 50 mL serum vial, pre-filled with saturated saline solution, samples were stored upside-down until analyzed in the laboratory by gas chromatography (GC; see below). Fluxes to the atmosphere were estimated from the change in concentrations using the following equation:

$$F = [(s \cdot V) / (mV \cdot S)] \cdot f, \quad (1)$$

where F is the flux in $\mu\text{mol m}^{-2} \text{d}^{-1}$, s is the slope in $\mu\text{atm min}^{-1}$, V is the volume of the chamber in liters (L), mV (molar volume) is the volume of 1 mol of gas in L atm mol $^{-1}$, S is the surface area of the floating chamber over the water in square meters, and f is the conversion factor from minutes to days (1 d = 1440 min; see Teodoru et al., 2010). Measurements were performed on drift, with the chamber flowing alongside the current. Whenever possible, flux chamber measurements were performed in both static and drift mode

with constant records of water velocity (relative to the chamber for static mode) and drift velocity to account for the enhanced gas exchange coefficient due to locally induced turbulence by the chamber itself. At each location, before and after chamber measurements, additional ambient air $p\text{CO}_2$ was measured by injecting air samples into the EGM-4 analyzer, while air temperature, barometric pressure, humidity and wind speed were measured at ~ 1 m above the water surface using a hand-held anemometer (Kestrel 4000, accuracy 3 %). Measurement precision of $p\text{CO}_2$ with the EGM-4 was ± 1 %, and the stability/drift of the instrument (checked after each trip) was always less than 2 %.

Samples for dissolved CH_4 , N_2O and the stable isotope composition of DIC ($\delta^{13}\text{C}_{\text{DIC}}$) were collected in 50 mL serum bottles (for CH_4 and N_2O) and 12 mL Exetainer vials (for $\delta^{13}\text{C}_{\text{DIC}}$) filled from the Niskin bottle (allowing water to overflow), poisoned with HgCl_2 , and capped without headspace. Concentrations of CH_4 and N_2O were determined by the headspace equilibration technique (20 mL N_2 headspace in 50 mL serum bottles) and measured by means of GC (Weiss, 1981) with flame ionization detection (GC-FID) and electron capture detection (GC-ECD) with a SRI 8610C GC-FID-ECD calibrated with CH_4 : CO_2 : N_2O : N_2 mixtures (Air Liquide, Belgium) of 1, 10 and 30 ppm CH_4 and of 0.2, 2.0 and 6.0 ppm N_2O , and using the solubility coefficients of Yamamoto et al. (1976) for CH_4 and Weiss and Price (1980) for N_2O . The overall precision of measurements was ± 4 % for CH_4 and ± 3 % for N_2O . For the analysis of $\delta^{13}\text{C}_{\text{DIC}}$, a 2 mL helium (He) headspace was created, and H_3PO_4 was added to convert all DIC species to CO_2 . After overnight equilibration, part of the headspace was injected into the He stream of an elemental analyzer–isotope ratio mass spectrometer (EA-IRMS, Thermo Finnigan Flash HT and Thermo Finnigan Delta V Advantage) for $\delta^{13}\text{C}$ measurements. The obtained $\delta^{13}\text{C}$ data were corrected for the isotopic equilibration between gaseous and dissolved CO_2 as described in Gillikin and Bouillon (2007), and measurements were calibrated with certified reference materials LSVEC and either NBS-19 or IAEA-CO-1.

For total alkalinity (TA), 80 mL of water samples was filtered on 0.2 μm polyethersulfone syringe filters (Sartorius, 16532-Q) and analyzed via automated electro-titration on 50 mL samples with 0.1 mol L $^{-1}$ HCl as titrant (reproducibility was typically better than ± 3 $\mu\text{mol L}^{-1}$ based on replicate analyses). DIC concentrations were computed from TA, water temperature and $p\text{CO}_2$ measurements using thermodynamic constants of Millero (1979) as implemented in the CO2SYS software (Lewis and Wallace, 1998). Using an estimated error for $p\text{CO}_2$ measurements of ± 1 %, ± 3 μM for TA and ± 0.1 °C for temperature, the propagated error for DIC is ± 5 %. The concentrations of calcium (Ca), magnesium (Mg) and dissolved silica (DSi) were measured using inductively coupled plasma-atomic emission spectroscopy (Iris Advantage, Thermo Jarrell Ash). Pelagic community respiration (R) rates were determined by quantifying the decrease in DO

(with the optical DO probe YSI-ODO) using triplicate 60 mL Winkler bottles incubated in a dark coolbox filled with water (to retain ambient temperature) for approximately 24 h. A respiratory molar oxidation ratio of 1.3 O₂ : C was used as the conversion rate from oxygen measurements into C (Richardson et al., 2013). Particulate primary production (*P*) rates in surface waters (i.e., not depth-integrated rates) were quantified in duplicate by determining the uptake of DIC after short-term (2–3 h) in situ incubations of river water during the day using 1 L polycarbonate bottles spiked with ¹³C-labeled sodium bicarbonate (NaH¹³CO₃). A subsample of the spiked water was sampled to measure the degree of ¹³C enrichment in the DIC pool. Samples for analysis of δ¹³C_{POC} were obtained at the start (natural abundance values) and end of the incubation by filtering a known volume of surface water on pre-combusted (overnight at 450 °C) 25 mm GF/F filters (0.7 μm). Filters were decarbonated with HCl fumes for 4 h, re-dried and then packed into Ag cups. Particulate organic carbon (POC) and δ¹³C_{POC} were determined on a Thermo EA-IRMS system (Flash HT with Delta V Advantage), using the thermal conductivity detector signal of the EA to quantify POC, and by monitoring *m/z* 44, 45 and 46 on the IRMS. Quantification and calibration of δ¹³C data were performed with IAEA-C6 and acetanilide that was calibrated against international standards. Reproducibility of δ¹³C_{POC} measurements was typically better than 0.2‰. Calculations to quantify the *P* rates were made as described by Dauchez et al. (1995). The *R* and *P* data here (in μmol C L⁻¹ h⁻¹) refer only to surface water (~0.5 m deep) measurements and not to depth-integrated values.

3 Results and discussion

3.1 Temporal and spatial variability of *p*CO₂

*p*CO₂ along the Zambezi River was highly variable, both spatially and temporally. Riverine *p*CO₂ was generally higher during wet seasons compared to the dry season (Fig. 3a). Lowest riverine values (i.e., excluding reservoirs) during the 2012 and 2013 wet seasons of 640 and 660 ppm, respectively, were found immediately below Victoria Falls, while highest concentrations were always recorded downstream of the Barotse Floodplain (7650 and 10 350 ppm, respectively) and downstream of the confluence with the Shire River in Mozambique (8180 and 12 200 ppm, respectively; Fig. 3a). During the dry season of 2013, the lowest concentration (300 ppm, i.e., below atmospheric equilibrium) was measured at ZBZ.6, while highest *p*CO₂ was found at the river source and immediately below the Kariba Dam (2550 and 2600 ppm, respectively; Fig. 3a). Mean *p*CO₂ for the entire river (i.e., excluding reservoirs) was 2475 and 3730 ppm, respectively, during the 2012 and 2013 wet seasons, but only 1150 ppm (measurements up to ZBZ.13 only) during the 2013 dry season. Despite relatively large interannual

variability (paired *t* test significantly different, *p* < 0.025, *n* = 15), but low seasonality (*p* < 0.09, *n* = 8), *p*CO₂ along the Zambezi followed the same longitudinal pattern (slightly different during the dry season; Fig. 3a). The *p*CO₂ was always below atmospheric equilibrium in the surface water of the two major reservoirs (mean for all campaigns: 267 ppm for Kariba and 219 ppm for Cahora Bassa) with no distinct interannual variability or seasonality (Fig. 3a).

Large variability of riverine *p*CO₂ was also observed for the Kafue River (Fig. 3b). Excluding reservoir values, *p*CO₂ along the Kafue River varied between 905 and 1145 ppm during the 2012 and 2013 wet seasons, respectively (both recorded at KAF.6 located immediately below the Itzhi Tezhi Dam), up to 9985 and 11 745 ppm, respectively (both measured at KAF.8 in the Kafue Flats). Concentrations were consistently lower during the dry season 2013, ranging from 330 ppm at KAF.4 (below the Lukanga Swamps) up to 6650 ppm at the end of the Kafue Flats (KAF.9; Fig. 3b). With mean *p*CO₂ for the entire river of 3805 and 4748 ppm, respectively (without the Itzhi Tezhi Reservoir), values in the Kafue were significantly different during the two wet season campaigns (paired *t* test, *p* < 0.009, *n* = 9) as well as during the 2013 dry season compared to the 2013 wet season (*p* < 0.026, *n* = 7, mean 2770 ppm). *p*CO₂ in the surface water of the Itzhi Tezhi Reservoir was always above atmospheric concentration during both wet seasons (mean 1130 ppm in 2012 and 1554 ppm in 2013), showing a decreasing pattern with increasing the distance from the river inflow. The only measurement during the 2013 dry season in the middle of the reservoir (ITT.2) indicated strong CO₂ undersaturated conditions (165 ppm). As observed for the Zambezi River, the variability of *p*CO₂ along the Kafue River followed a similar pattern during each campaign.

Overall, there was a relatively good (*r*² = 0.78) negative correlation between CO₂ (μmol L⁻¹) and DO concentration (μmol L⁻¹) for all sampled rivers, tributaries and reservoirs, and during all campaigns (Fig. 3c), with mostly reservoir samples characterized by high DO and low CO₂ content, while hypoxic conditions associated with high CO₂ values were characteristic of the Shire River and several stations on the Zambezi and the Kafue rivers (mostly downstream of the floodplains). The slope of this relationship of 0.79 ± 0.04 could provide an estimate of the respiratory quotient (RQ), defined as the molar ratio of O₂ consumed to CO₂ produced by respiration. The RQ value is in theory equal to 1 for the oxidation of glucose, but is higher than 1 for more complex and reduced organic molecules containing nitrogen and phosphorus, such as lipids and proteins, or lower than 1 for highly oxidized and oxygen-rich molecules (e.g., pyruvic, citric, tartaric, and oxalic acids; Berggren et al., 2012). The value we computed is lower than the RQ value of 1.3 established in a temperate stream with a catchment dominated by pastures (Richardson et al., 2013) but close to the one recently proposed for bacterial respiration in boreal lakes of 0.83 (Berggren et al., 2012). Berggren et al. (2012) attribute

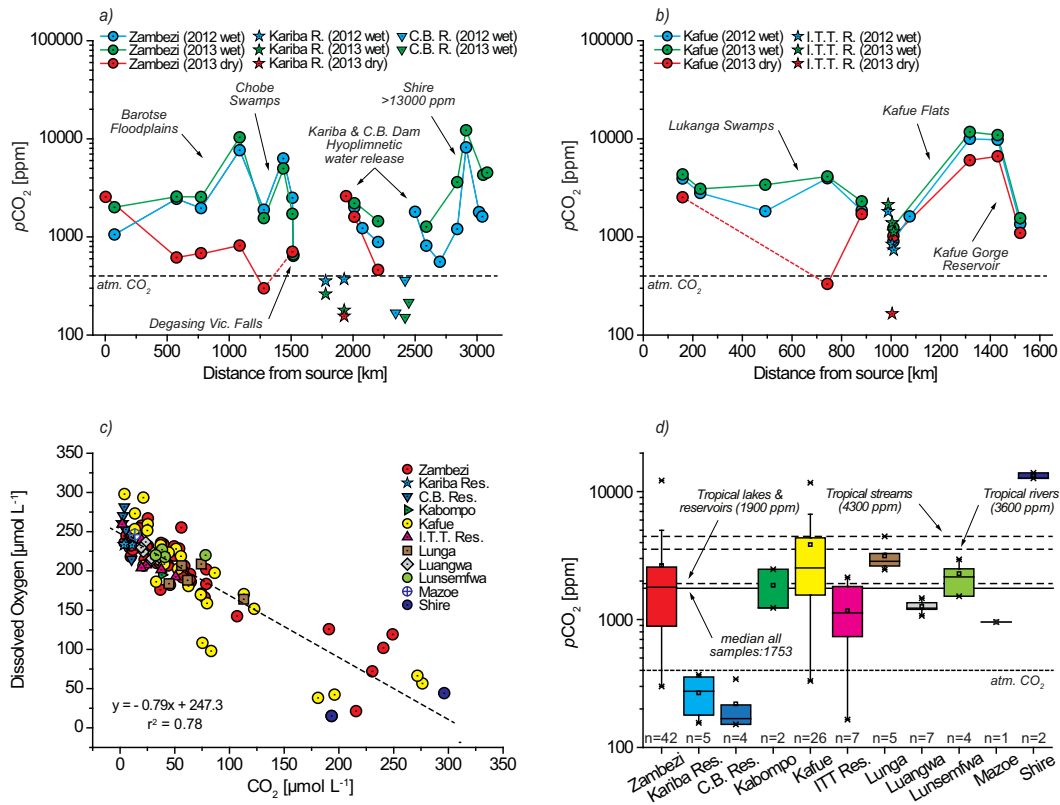


Figure 3. Spatial and temporal variability of $p\text{CO}_2$ along (a) the Zambezi River, including the Kariba Reservoir (Kariba R.) and Cahora Bassa Reservoir (C. B. R.), and (b) the Kafue River, including the Itezhi Tezhi Reservoir (I. T. T. R.). Panel (c) shows the negative correlation between CO_2 and dissolved oxygen ($\mu\text{mol L}^{-1}$). Panel (d) shows the overall range in $p\text{CO}_2$ for the Zambezi River, tributaries and reservoirs. Box plots show range, percentile, median, mean and outliers. The dotted line represents atmospheric CO_2 concentration, while dashed lines represent global median $p\text{CO}_2$ values for tropical rivers, streams and lakes/reservoirs based on Aufdenkampe et al. (2011). The solid line represents the median $p\text{CO}_2$ value (1753 ppm) of all sites during the entire sampling period.

this low RQ to the bacterial degradation of highly oxidized molecules such as organic acids, likely to be also abundant at our sampling sites (Lambert et al., 2015).

With an overall mean of 2639 ppm over the entire sampled period (both wet and dry), $p\text{CO}_2$ of the Zambezi River was 45 % lower than mean $p\text{CO}_2$ of the Kafue River (mean 3852 ppm; Fig. 4d). All other tributaries also displayed CO_2 supersaturated conditions with respect to atmospheric equilibrium with mean values ranging from as low as 955 and 1402 ppm in the Mazoe and the Luangwa rivers and up to 13 351 ppm in the Shire River (Fig. 4d). While mean values of the two large reservoirs on the Zambezi River indicate undersaturated CO_2 conditions, overall mean $p\text{CO}_2$ of the much smaller Itezhi Tezhi Reservoir on the Kafue River of 1174 ppm was well above atmospheric equilibrium (Fig. 4d).

3.2 Temporal and spatial variability of CH_4

CH_4 along the Zambezi also showed a relatively large spatial heterogeneity but low temporal variability (Fig. 4a). Lowest CH_4 concentrations during the two wet season campaigns

(2012 and 2013) of 7 and 13 nmol L^{-1} , respectively, were both recorded at station ZBZ.9 immediately below Victoria Falls. The highest value of the 2012 wet season campaign of 2394 nmol L^{-1} was measured at ZBZ.17, while the highest CH_4 concentration of the 2013 wet season of 12 127 nmol L^{-1} was recorded at station ZBZ.5, downstream of the Barotse Floodplain (Fig. 4a). Mean value of the 2012 wet season campaign of 623 nmol L^{-1} was 2-fold lower than mean CH_4 of the 2013 wet season (1216 nmol L^{-1} driven by the extremely high value at station ZBZ.5), but median (348 and 274 nmol L^{-1} for the 2012 and 2013 wet seasons, respectively) and statistical analyses (paired t test, $p > 0.516$, $n = 15$) suggest no significant interannual variability. In the absence of comparative measurements at station ZBZ.9 below Victoria Falls, lowest CH_4 concentration along the Zambezi during the 2013 dry season campaign of 25 nmol L^{-1} was recorded at ZBZ.10 in the Kariba Gorge (4 km downstream of the Kariba Dam), whereas maximum value of 874 nmol L^{-1} was measured at ZBZ.5, downstream of the Barotse Floodplain (Fig. 4a). Although the mean CH_4 of the 2013 dry season of 361 nmol L^{-1} was much lower than the

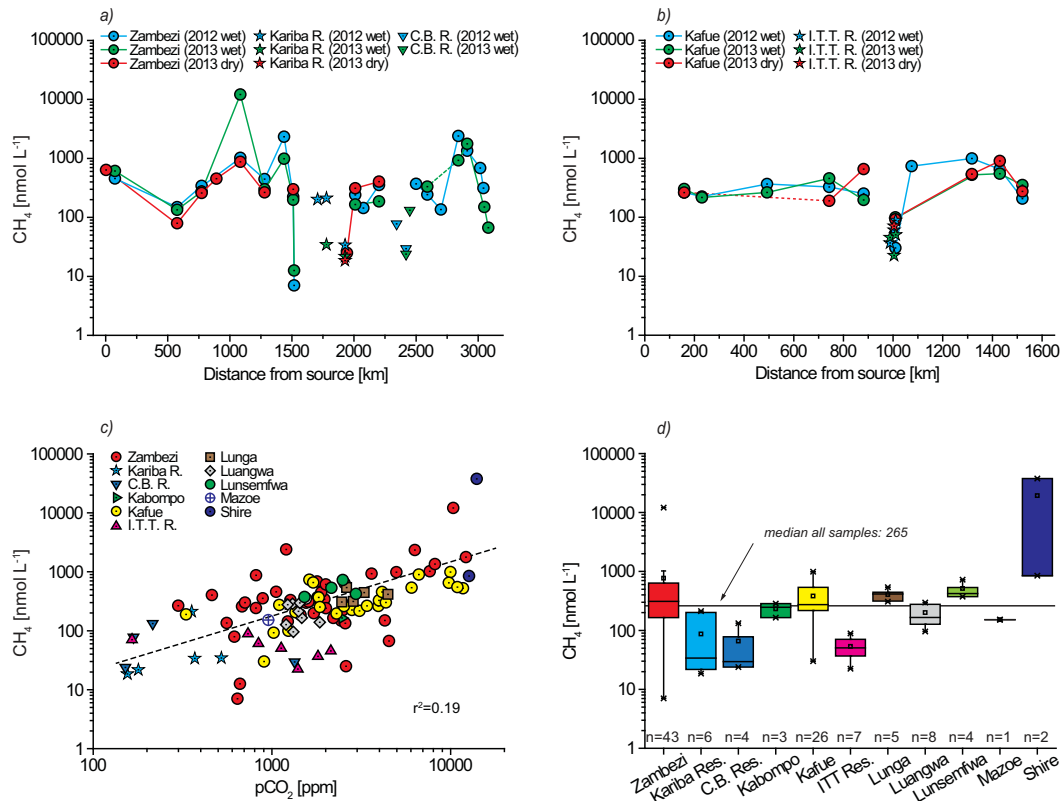


Figure 4. Spatial and temporal variability of CH₄ along (a) the Zambezi mainstem, including the Kariba Reservoir (Kariba R.) and Cahora Bassa Reservoir (C. B. R.), and (b) the Kafue River, including the Itezhi Tezhi Reservoir (I. T. T. R.). Panel (c) shows the correlation between CH₄ and pCO₂. Panel (d) shows the overall (all campaigns) range of CH₄ concentration for the Zambezi River, tributaries and reservoirs. Box plots show range, percentile, median, mean and outliers. The solid line represents the median CH₄ value (265 μmol L⁻¹) of all sites during the entire sampling period.

equivalent mean of the 2013 wet season campaign, its median value of 305 nmol L⁻¹ and the paired *t* test ($p > 0.368$, $n = 8$) indicate little CH₄ seasonality along the Zambezi River. CH₄ concentrations in the surface water of the two reservoirs on the Zambezi were generally lower compared to the riverine values and consistently below levels measured at the stations immediately downstream of both dams (Fig. 4a). Concentrations in the Kariba were higher during the 2012 wet season (mean 149 nmol L⁻¹) compared to the 2013 wet season (mean 28 nmol L⁻¹) but opposite in the Cahora Bassa (mean 54 and 78 nmol L⁻¹, respectively). The only CH₄ measurement in the Kariba Reservoir during the 2013 dry season reached 19 nmol L⁻¹ (Fig. 4a).

Relatively low temporal variability of CH₄ (both interannual and seasonal) was also observed along the Kafue River (Fig. 4b), where concentrations varied from minimums of 30, 100 and 92 nmol L⁻¹ during the 2012 and 2013 wet seasons and the 2013 dry season, respectively (all recorded at KAF.6, immediately below the Itezhi Tezhi Dam), to a maximum of 992, 550 and 898 nmol L⁻¹ during the same period at the two stations in the Kafue Flats (KAF.8 and KAF.9). With mean CH₄ values of 405, 329 and 416 nmol L⁻¹ (or

median 298, 302 and 274 nmol L⁻¹) for the 2012 and 2013 wet seasons and the 2013 dry season, respectively, CH₄ concentrations along the Kafue were not statistically different during the 2012 wet season compared to the 2013 wet season (paired *t* test, $p > 0.541$, $n = 9$), nor during the 2013 wet and dry seasons ($p > 0.543$, $n = 7$). CH₄ concentrations in the surface water of the Itezhi Tezhi Reservoir were generally lower than riverine values, ranging between 37 and 89 nmol L⁻¹ (mean 62 nmol L⁻¹) during the 2012 wet season, and 22 and 51 nmol L⁻¹ (mean 40 nmol L⁻¹) during the 2013 wet season (Fig. 4b). The only CH₄ measurement during the 2013 dry season in the Itezhi Tezhi Reservoir (ITT.2) reached 71 nmol L⁻¹.

There was an overall positive, albeit weak ($r^2 = 0.186$, $n = 106$), correlation between CH₄ and pCO₂ (log–log scale) for all rivers, tributaries and reservoirs, and all campaigns, with values at the lowest end mostly characteristic of the Kariba and Cahora Bassa reservoirs, and the higher end occupied by the Shire River and several stations on the Zambezi and Kafue rivers located in or downstream of major floodplains/wetlands (Fig. 4c). With an arithmetic average value (all samples) of 769 nmol L⁻¹ for the entire sam-

pled period, CH₄ of the Zambezi River was twice as high as the equivalent average CH₄ concentration of the Kafue River (mean 381 nmol L⁻¹; Fig. 4d). With the exception of the Shire River which displayed extremely high concentrations (mean 19 328 nmol L⁻¹ based on only two measurements), all other tributaries of the Zambezi River had a similar mean CH₄ level ranging from 200 nmol L⁻¹ in the highly turbid Luangwa River up to 514 nmol L⁻¹ in the Lunsemfwa River (tributary of Luangwa; Fig. 4d). CH₄ concentrations in the surface water of all three reservoirs were comparable (mean 87, 66 and 54 nmol L⁻¹ for Kariba, Cahora Bassa and Itezhi Tezhi, respectively) and generally lower than riverine values (Fig. 4d). With the exception of the Itezhi Tezhi, CH₄ values measured at stations immediately below both Kariba and Cahora Bassa dams were substantially higher compared to levels characterizing the surface water of the two reservoirs

3.3 Temporal and spatial variability of N₂O

N₂O in the Zambezi River was also characterized by high spatial variability. During both the 2012 and 2013 wet season campaigns, N₂O along the Zambezi ranged from 4.1 nmol L⁻¹ at ZBZ.5 (downstream of the Barotse Floodplain) and 2.9 nmol L⁻¹ at ZBZ.18 (downstream of the confluence with the Shire River) up to 8.5 and 8.0 nmol L⁻¹, respectively, both at ZBZ.11, downstream of the Kariba Dam (Fig. 5a). Higher overall concentrations but lower spatial variability was recorded during the 2013 dry season, when concentrations ranged between 7.9 nmol L⁻¹ at ZBZ.13 (upstream of the Cahora Bassa Reservoir) and 11.4 nmol L⁻¹ at ZBZ.10 (downstream of the Kariba Dam; Fig. 5a). Statistical analyses of N₂O concentrations of the two wet season campaigns (mean 6.7, and 6.1 nmol L⁻¹ for 2012 and 2013, respectively) and the 2013 dry season (mean 8.8 nmol L⁻¹) suggest low interannual variability (paired *t* test, *p* > 0.142, *n* = 15) but strong N₂O seasonality (paired *t* test, *p* < 0.0004, *n* = 8) along the Zambezi River mainstem. The only measurement during the 2013 dry season in the surface water of the Kariba Reservoir suggests that N₂O was also higher (mean 8.6 nmol L⁻¹) compared to values of the 2012 and 2013 wet seasons (mean 6.3 and 6.5 nmol L⁻¹, respectively). The same high spatial heterogeneity and low N₂O interannual variability was observed along the Kafue River, where values of the 2012 and 2013 wet seasons (mean 5.9 and 5.7 nmol L⁻¹, respectively) were not statistically different (paired *t* test, *p* > 0.549, *n* = 9). It is worth noting that both minimum N₂O values of the two consecutive wet season campaigns (3.9 and 3.0 nmol L⁻¹, respectively) were recorded at station KAF.8 in the Kafue Flats. Ranging from 7.0 nmol L⁻¹ in the Kafue Flats to 10.3 nmol L⁻¹ at the headwater station (KAF.1), N₂O during the 2013 dry season (mean 8.4 nmol L⁻¹) was significantly higher (paired *t* test, *p* < 0.001, *n* = 7) compared to the 2013 wet season. N₂O values in the surface water of the Itezhi Tezhi Reservoir were

similar during both wet season campaigns (mean 6.8 and 6.5 nmol L⁻¹, respectively) and slightly higher than riverine values. Only one N₂O measurement in the Itezhi Tezhi during the 2013 dry season (at ITT.2) reached 7.8 nmol L⁻¹ (Fig. 5b).

There was an overall good (*r*² = 0.48) and negative correlation between N₂O and *p*CO₂ (Fig. 5c), with high N₂O concentrations and low *p*CO₂ mostly characteristic of reservoirs and riverine stations downstream of dams, while low N₂O and high *p*CO₂ were characteristic of the Shire River and stations on the Zambezi and Kafue downstream of the floodplains. There was no correlation between N₂O and NH₄⁺ or NO₃⁻, while a positive relation with %DO was only found during wet seasons (data not shown). Despite seasonal and longitudinal variations, mean N₂O values were relatively similar among tributaries, with little variability (means from 6.2 for the Lunga to 7.5 nmol L⁻¹ for the Lunsemfwa), with the exception of the Shire River, which was characterized by a distinctly lower value (mean 2.7 nmol L⁻¹; Fig. 5d). N₂O values in the surface water of the Kariba and the Cahora Bassa reservoirs (mean 6.8 and 7.3 nmol L⁻¹, respectively) were close to riverine values (Fig. 5d).

3.4 Patterns in GHG dynamics along the river continuum

As shown above, dissolved GHG concentrations along the Zambezi and the Kafue rivers display large spatial heterogeneity. However, concentrations followed similar longitudinal patterns during both consecutive wet season campaigns and were only slightly different during the dry season, which can be attributed to the connectivity between river and floodplains/wetlands, the input from major tributaries, and the presence of natural or anthropogenic barriers (waterfalls/rapids and reservoirs) along the aquatic continuum. We will examine these patterns in detail using the example of *p*CO₂ during the 2012 wet season campaign since this represents the most complete data set (Fig. 3a).

Starting at an initial 1055 ppm at the Zambezi source (ZBZ.1), *p*CO₂ increased downstream to about 2450 ppm at ZBZ.2 as the river traverses a low gradient area, receiving water from the Chifumage and Luena tributaries, which drain large floodplains in SE Angola. After a small decrease to 1970 ppm downstream of the confluence with the Kabompo River (ZBZ.3), *p*CO₂ increased sharply to over 7650 ppm at ZBZ.5 (ZBZ.4 was not sampled during wet season) as the river exchanges waters with the Barotse Floodplain. This high CO₂ load, associated with low pH (6.97) and %DO (47 %, Table S1 in the Supplement), was rapidly outgassed downstream due to a sharper gradient of this river sector which forms several rapids and the 14 m high Ngonye Falls, reaching only 1980 ppm at ZBZ.6. Further downstream, *p*CO₂ peaked again (> 6300 ppm at ZBZ.7) as the river passes through the Caprivi–Chobe Swamps, but dropped quickly down to 2500 ppm upstream of Victoria

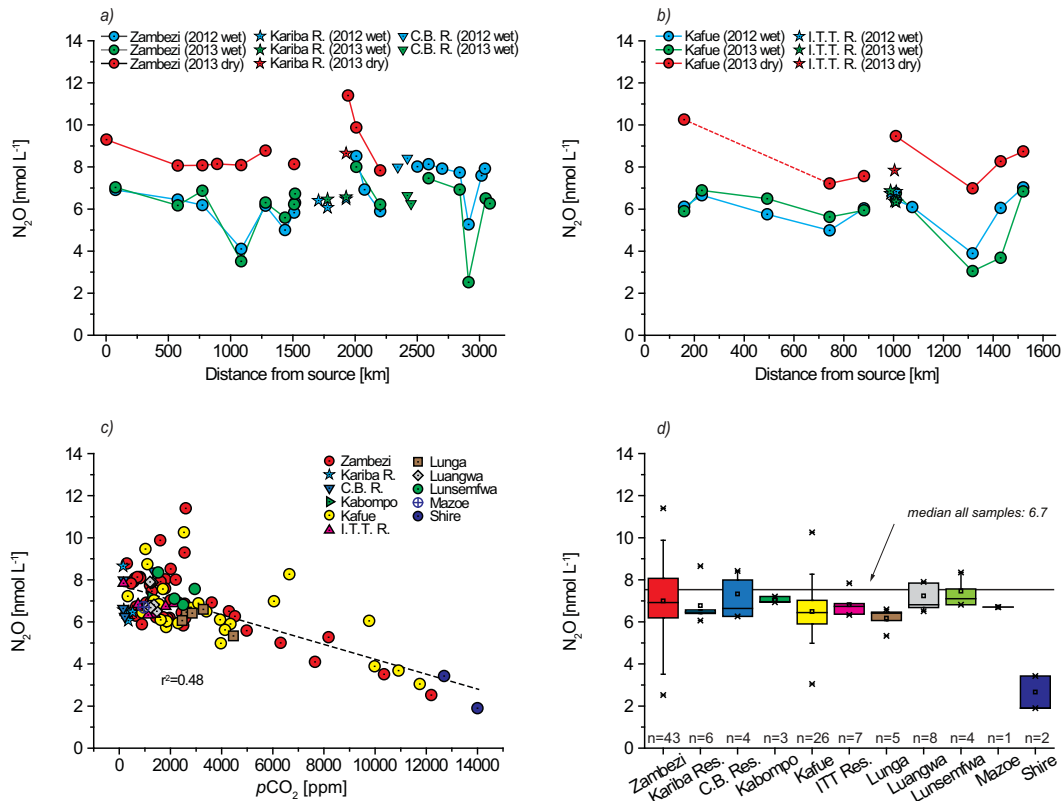


Figure 5. Spatial and temporal variability of N_2O along (a) the Zambezi River, including the Kariba Reservoir (Kariba R.) and Cahora Bassa Reservoir (C. B. R.), and (b) the Kafue River, including the Itezhi Tezhi Reservoir (I. T. T. R.). Panel (c) shows the correlation between N_2O and $p\text{CO}_2$. Panel (d) shows overall (all campaigns) range N_2O concentration for the Zambezi River, tributaries and reservoirs. Box plots show range, percentile, median, mean and outliers. The solid line represents median N_2O value ($6.7 \mu\text{mol L}^{-1}$) of all sites during the entire sampling period.

Falls (ZBZ.8) due to the further steepening of the river gradient and the enhanced turbulent flow over the Mambova and the Katombora Rapids. As the river plunged down over 100 m height of Victoria Falls, there was an instant and almost complete CO_2 outgassing, with river waters approaching atmospheric equilibrium at the base of the falls (642 ppm at ZBZ.9). Downstream of Victoria Falls, the river experiences a turbulent flow through the narrow, 100 km long Bataoka Gorge and the Chimba Rapids, and CO_2 is expected to decrease further, approaching atmospheric concentrations at the inflow of the Kariba Reservoir. These CO_2 -depleted inflow waters combined with CO_2 uptake by primary production (mean $P \sim 16.6 \mu\text{mol C L}^{-1} \text{h}^{-1}$) could be put forward to explain the CO_2 undersaturated conditions encountered in the surface waters of the Kariba Reservoir throughout all campaigns (Fig. 3a). In contrast to the CO_2 undersaturated (and warmer, DO-saturated) epilimnetic conditions of the Kariba Reservoir, much higher $p\text{CO}_2$ (> 2000 ppm, accompanied by colder water and undersaturated DO conditions) measured 70 km downstream of the Kariba Dam (at ZBZ. 11) suggests the discharge at the dam of hypolimnetic, low-DO and CO_2 -loaded waters, formed as a result

of thermal stratification of the water column of the reservoir (Kunz et al., 2011a). Even though no major tributaries or other point sources (i.e., wetlands) exist along this 70 km stretch, the potential contribution of lateral sources to the $p\text{CO}_2$ measured at ZBZ.11 cannot be completely ruled out. However, measurements during 2013 dry campaign showed a constant decrease in $p\text{CO}_2$ (and an increase in %DO and water temperature) between the intermediate point ZBZ.10 (located 17 km downstream of the dam) and ZBZ.11 from 2600 ppm (65 % DO and 24.1°C) to 1600 ppm (82 % DO and 24.3°C), respectively. This higher upstream $p\text{CO}_2$ level at ZBZ.10 and the steady downstream decrease (accompanied by increase in %DO and water temperature) support the idea of hypolimnetic water discharge with high $p\text{CO}_2$, which, even if partially decreased due to CO_2 efflux to the atmosphere, is still reflected in the $p\text{CO}_2$ measured 70 km downstream at ZBZ.11. Low re-aeration rates with hypoxic conditions caused by periodically hypolimnetic water discharge have been previously described to last for more than 100 km downstream of the Itezhi Tezhi Dam (Kunz et al., 2013). A simple calculation based on a mass balance approach which assumes no additional lateral CO_2 source along

this 70 km stretch and uses the CO₂ concentrations and fluxes measured at ZBZ.11 during all three sampling campaigns, together with the daily discharge rates at Kariba Dam, suggests that *p*CO₂ at the outlet of the reservoir would vary between 3500 and 4600 ppm. Even these estimated figures may be in fact slightly higher since the (low) fluxes at ZBZ.11 are not representative of the entire 70 km stretch (especially for the narrow and steep Kariba Gorge section), they are still substantially lower compared to *p*CO₂ ranges measured in the hypolimnion of several tropical reservoirs (Gu erin et al., 2006).

Riverine *p*CO₂ decreased further downstream of site ZBZ.11 through CO₂ efflux to the atmosphere, favored by the substantial broadening of the river sector, reaching 1230 ppm at ZBZ.12 and 890 ppm at ZBZ.13. *p*CO₂ in the surface water of the Cahora Bassa Reservoir was below atmospheric equilibrium (168 and 342 ppm) and generally similar to those measured in the Kariba. As in the case of Kariba, *p*CO₂ measured 40 km downstream of the Cahora Bassa Dam (at ZBZ.14) of 1800 ppm (and 340 nmol L⁻¹ CH₄ compared to ~50 nmol L⁻¹ in the surface water of the reservoir) suggests the discharge of hypolimnetic water through the bottom intake with high CO₂ (and CH₄) content. *p*CO₂ decreased further downstream of the dam due to the turbulent flow throughout the narrow Cahora Bassa Gorge and the broadening of the river section towards the coastal plains, reaching 815 and 560 ppm at ZBZ.15 and ZBZ.16, respectively. Further downstream, *p*CO₂ increased up to 1205 ppm (at ZBZ.17), most probably influenced by the wide riparian wetlands/marshes along the river banks, and increased further downstream to over 8180 ppm at ZBZ.17 as the Zambezi River receives waters from the highly CO₂-oversaturated Shire River (12 700 ppm CO₂, 17.3 % DO), which drains a stagnant water complex of swamp/marshes (known as the Elephant Marsh). This high CO₂ load was slowly exchanged with the atmosphere towards the delta, with river *p*CO₂ reaching 1790 ppm at ZBZ.19 and 1610 ppm at ZBZ.20 close to the river mouth (Fig. 3a).

This longitudinal pattern of *p*CO₂ along the Zambezi River described above was closely repeated during the second wet season campaign (Fig. 3a). Despite the overall lower values during the 2013 dry season, *p*CO₂ also followed a relatively similar pattern, reflecting also the influence of the Barotse Floodplain (although less pronounced), the quick CO₂ outgassing downstream due to the presence of several rapids and the Ngonye Falls, and the influence of the Chobe Swamps (Fig. 3a). The only obvious difference relative to the wet seasons occurred in the Zambezi headwaters when *p*CO₂ decreased substantially between the source station ZBZ.1 and ZBZ.2 compared to the increased pattern observed during both wet seasons. This could be potentially explained by the reduction of lateral input load as a result of loss of connectivity between the river and the riparian wetlands associated with lower water level during the dry season.

Similar longitudinal patterns, reflecting the influence of wetlands, reservoirs, and waterfalls/rapids along the Zambezi mainstem, were also observed for CH₄ (Fig. 4a) as well as for N₂O, with the latter showing a mirror image of the patterns in *p*CO₂ (Fig. 5a). The positive relationship between CH₄ and CO₂ suggests that both are largely controlled by organic matter degradation processes. The negative relationship between N₂O and *p*CO₂ and the positive relationship between N₂O and %DO suggests, on the other hand, that N₂O is removed by denitrification in the sediments. Low N₂O levels have been also observed in the Amazon floodplains (Richey et al., 1988) and in the hypolimnion of anoxic lakes (Mengis et al., 1997).

The influence of wetlands/floodplains and reservoirs on the dynamics of *p*CO₂ can be also seen along the Kafue River (Fig. 3b), where a steady increase in *p*CO₂ values was recorded during both wet seasons (2012 and 2013) at station KAF.4 below the Lukanga Swamps as well as in and downstream of the Kafue Flats (KAF.7, KAF.8, KAF.9; Fig. 3b). The different pattern (decrease instead of increase) during the 2013 dry season for the upper Kafue (upstream of the Itezhi Tezhi Reservoir) can be explained by the loss of connectivity between river mainstem and the swamps. Low water levels during the 2013 dry season, which partially exposed the river bedrock along this stretch, enhanced the turbulent flow (and subsequently the gas exchange coefficient) as suggested by oversaturated DO value (143 %), lowering the *p*CO₂ level close to atmospheric equilibrium. In the absence of an important lateral CO₂ source, photosynthetic CO₂ uptake by primary production higher than in the Kariba Reservoir ($P \sim 21.8 \mu\text{mol C L}^{-1} \text{ h}^{-1}$) should have further reduced the CO₂ down to undersaturated conditions. The peculiar situation downstream of the Itezhi Tezhi Reservoir, where riverine *p*CO₂ also showed an increase in and downstream of the Kafue Flats during the 2013 dry season campaign, can be explained by the specific hydrology of the flats altered by the operation of the two bordering dams. The completion of the Kafue Gorge Dam in 1972 led to an average rise in water table of over 2 m in the lower Kafue Flats which created a permanently flooded area of over 800 km² (McCartney and Houghton-Carr, 1998). Completed in 1978 with the purpose of upstream storage in order to ensure constant water supply for the Kafue Gorge Dam, the Itezhi Tezhi Reservoir further altered the hydrology of the Kafue Flats. Triggered by rising energy demands, substantial increases in flow have been implemented at the Itezhi Tezhi Dam during dry seasons, while flood peaks have partly been delayed and attenuated, changing the timing and extent of flooding in the Kafue Flats (Mumba and Thompson, 2005). This hydrological alteration due to river damming, responsible for the creation of a permanent flooded area within the Kafue Flats which constantly exchanges water with the Kafue River mainstem, could explain the observed high riverine *p*CO₂ levels encountered there also during the 2013 dry season (Fig. 3b). In contrast to the Zambezi River, where riverine CO₂ concentrations down-

stream of both dams were significantly higher compared to those in the surface water reservoirs, $p\text{CO}_2$ values at KAF.6, immediately downstream of the dam, were similar to those measured in the epilimnion of the Itezhi Tezhi Reservoir (Fig. 3b). Unlike Kariba and Cahora Bassa, the Itezhi Tezhi Dam was not designed for power production, with water being released from the epilimnion over the spillways, and rare bottom water withdrawals only during low storage (Zurbrügg et al., 2012). For the Kafue Gorge Reservoir, since no measurements were carried out in or immediately below the dam, we can only speculate the existence of a large CO_2 pool, both in the epilimnion and hypolimnion of the reservoir (given the inflow concentrations of over 9000 ppm – at KAF.9) and the release of large amounts of GHGs to the river downstream. We can further speculate that much lower $p\text{CO}_2$ levels measured systematically at KAF.10 (65 km downstream of the dam) compared to upstream stations (Fig. 3b) are the effect of rapid outgassing of hypolimnetic $p\text{CO}_2$ through the narrow and steep Kafue Gorge (600 m drop over less than 30 km).

All abovementioned effects of wetlands, reservoirs and the distinct hydrology on the dynamics of CO_2 concentrations along the Kafue River can also explain the longitudinal patterns of CH_4 and N_2O and, in combination with the hydrological conditions which determine the degree of water exchange with floodplains, are responsible for part of their temporal variability (Fig. 4b, c).

$p\text{CO}_2$ values of all our sampled rivers and streams were generally well above atmospheric concentrations and comparable with $p\text{CO}_2$ values observed in other African rivers (i.e., the Tendo, Aby, Oubangui, Tana and Athi–Galana–Sabaki rivers; see Koné et al., 2009; Bouillon et al., 2009, 2014; Tamooch et al., 2013; Marwick et al., 2014). However, values were well below global levels of tropical rivers and streams given by Aufdenkampe et al. (2011; median 3600 and 4300 ppm, respectively), except for the Shire River (mean and median 13 350 ppm, $n = 2$; Fig. 3d). This may be explained by the fact that global CO_2 levels for tropical aquatic systems originates mostly from studies on the Amazon River basin, where “blackwater” rivers prevail. With $p\text{CO}_2$ in the surface water of the Itezhi Tezhi Reservoir above atmospheric concentration (mean 1174, median 1127 ppm), and substantially higher than both the Kariba (mean 267, median 275 ppm) and Cahora Bassa reservoirs (mean 219, median 192 ppm), its level was still lower than literature-based median value for tropical lakes and reservoirs of 1900 ppm suggested by Aufdenkampe et al. (2011; Fig. 3d). Undersaturated CO_2 conditions in surface waters such as the Kariba and the Cahora Bassa reservoirs have been previously described for other reservoirs in Africa (Bouillon et al., 2009; Tamooch et al., 2013). Overall, CH_4 concentrations in the Zambezi River mainstem (mean 769 nmol L^{-1}), higher than those of its major tributaries and reservoirs (Fig. 4d), were on average much higher than those measured in other African river systems such as the Oubangui River ($\sim 160 \text{ nmol L}^{-1}$; Bouillon et al., 2014), the Tana River ($\sim 160 \text{ nmol L}^{-1}$;

Bouillon et al., 2009), the Galana River and several streams in Kenya (250 and 180 nmol L^{-1} , respectively; Marwick et al., 2014), and three rivers in Côte d’Ivoire (Comoé: 206 nmol L^{-1} ; Bia: 238 nmol L^{-1} ; and Tanoé: 345 nmol L^{-1} ; Koné et al., 2010). A comparable range was also observed in tributaries of the Oubangui ($\sim 740 \text{ nmol L}^{-1}$, Bouillon et al., 2014) and in the Athi–Galana–Sabaki river system in Kenya ($\sim 790 \text{ nmol L}^{-1}$; Marwick et al., 2014). With the exception of the Shire River, where low N_2O concentrations of $\sim 2.7 \text{ nmol L}^{-1}$ could be explained by denitrification, the mean N_2O range in the Zambezi River basin (6.2–7.5 nmol L^{-1} ; Fig. 5d) was similar to that of the Oubangui River mainstem and its tributaries (7.5 and 9.9 nmol L^{-1} , respectively; Bouillon et al., 2009). However, locally elevated concentrations linked to high anthropogenic N inputs have been recorded in the Athi–Galana–Sabaki river system in Kenya (up to 26 nmol L^{-1} ; Marwick et al., 2014).

3.5 Dissolved inorganic carbon and its stable isotope signature

DIC in freshwater can be differentiated into two fractions with distinct origins and behaviors: carbonate alkalinity, mostly in the form of bicarbonate ions (HCO_3^-), which comes from soil and bedrock weathering, and dissolved CO_2 , which results from respiration in soils, groundwaters, river sediments and waters column (Meybeck, 1987; Amiotte-Suchet et al., 1999). As the relative proportion of the two DIC fractions (and concentrations) depends greatly on the lithology of the drainage basin, rivers draining carbonate-rich watersheds would typically have high DIC concentrations (well above 1 mmol L^{-1}), of which HCO_3^- represents the major fraction compared to dissolved CO_2 (Meybeck, 1987). In these hard waters, characterized by high pH and high conductivity, HCO_3^- contributes to the majority of the TA. In contrast, rivers draining non-carbonate rocks and/or soils with high organic content would have lower DIC concentrations (well below 1 mmol L^{-1}), of which dissolved CO_2 commonly represents the dominant fraction (Abril et al., 2015). Characterized by low pH and low conductivity, these acidic, organic-rich waters (soft or black waters) generally contain high DOC levels, sometimes exceeding DIC concentrations (Rantakari and Kortelainen, 2008; Whitfield et al., 2009; Einola et al., 2011), and organic acid anions contribute importantly to the TA (Driscoll et al., 1989; Hemond, 1990; Hunt et al., 2011; Abril et al., 2015).

The DIC values in all our sampled rivers (mean 1.32 mmol L^{-1}) together with conductivity (mean 140 $\mu\text{S cm}^{-1}$) and pH values (mean 7.61) may suggest the carbonate-rich lithology of the basin. However, low DIC, pH and conductivity values in the headwaters and their increasing patterns downstream along both the Zambezi and the Kafue rivers during all campaigns (data in the Supplement) suggest either different chemical weathering rates and/or that a proportion of HCO_3^- may also come

from silicate rock weathering. This is also suggested by the overall good correlation of TA with the sum of Ca^{2+} and Mg^{2+} ($r^2 = 0.84$; Fig. 6a) and the rather weak relationship ($r^2 = 0.18$) with DSi (Fig. 6b). To distinguish between the contribution of silicate and carbonate weathering to the HCO_3^- , we applied the simple stoichiometric model of Garrels and Mackenzie (1971), which calculates the contribution of carbonate weathering (TA_{carb}) to TA from Ca^{2+} and Mg^{2+} as well as the contribution of silicate weathering (TA_{sil}) to TA from DSi according to

$$\text{TA}_{\text{carb}} = 2 \cdot \left(\left[\text{Ca}^{2+} \right] + \left[\text{Mg}^{2+} \right] - \left[\text{SO}_4^{2-} \right] \right), \quad (\text{R1})$$

$$\text{TA}_{\text{sil}} = [\text{DSi}]/2. \quad (\text{R2})$$

While SO_4^{2-} in Reaction (1) allows for Ca^{2+} originating from dissolution of gypsum (CaSO_4) to be accounted for, its contribution was ignored due to the absence of SO_4^{2-} measurements. However, occurrence of gypsum in the Zambezi Basin is sporadic and mostly as nodules in a clay-rich dambo within the Kafue Flats (Briggs and Mitchell, 1991) and in the upper catchment of Shire River (downstream of Lake Malawi; Ashton et al., 2001). We acknowledge that the approach used is prone to several caveats, such as the occurrence of weathering of Mg-rich silicates such as olivine or the presence of SO_4^{2-} derived from the oxidation of pyrite or elemental sulfur in organic sediments. However, it is difficult to fully address these issues given, for instance, the lack of information on the lithology of catchment, and a more in depth investigation of rock weathering is beyond the scope of the present study.

Nevertheless, application of the Garrels and Mackenzie (1971) model shows a significant positive relationship between the modeled TA ($\text{TA}_{\text{carb}} + \text{TA}_{\text{sil}}$) and observed TA ($r^2 = 0.87$, $n = 103$) for all measured tributaries, reservoirs and Zambezi mainstem samples, with most of the data points falling on the 1 : 1 line (Fig. 7a). The exception to this pattern is found on the uppermost two sites of the Kafue River (KAF.1 and KAF.2) during 2013 dry campaign, where modeled TA is twice as high as the observed TA (Fig. 7a) due to unusually high Ca^{2+} (1860 and 1360 μM) and Mg^{2+} (1035 and 1250 μM). Such high values during the low-flow period, also linked to low pH (around 6) and low conductivity (5.4 and 33 $\mu\text{S cm}^{-1}$, respectively), found in this area of intense mining activities (mostly copper and cobalt) could be the result of effluent discharge from the processing plants or leaking of contaminated water from the extraction pits, tailings and slag dumps. The contribution of carbonate rock weathering estimated as the percentage of TA_{carb} ($\% \text{TA}_{\text{carb}}$) to the total modeled TA ($\text{TA}_{\text{carb}} + \text{TA}_{\text{sil}}$) in all samples ranged between 28 and 97 % (mean 88 %; Fig. 7b). The strong ($r^2 = 0.88$), positive, exponential relationship between $\% \text{TA}_{\text{carb}}$ and TA (Fig. 7b), and the general increase in $\% \text{TA}_{\text{carb}}$ along the Zambezi mainstem (data not shown) may

indicate a lower contribution of carbonate rock weathering in the more humid forest areas of the northwestern basin compared to the mostly open grassland areas and savannah in the south and towards the ocean.

$\delta^{13}\text{C}_{\text{DIC}}$ in aquatic systems varies over a large range, being primarily controlled by both in-stream and watershed processes (Finlay and Kendall, 2007). Marine carbonates have a $\delta^{13}\text{C}$ close to 0 ‰, whereas $\delta^{13}\text{C}$ of atmospheric CO_2 is about -7.5 ‰ (Mook et al., 1983). The $\delta^{13}\text{C}$ of soil CO_2 depends on the signature of the organic matter being mineralized, and is expected to lie within the range bracketed by $\delta^{13}\text{C}$ signatures for C3 (~ -28 ‰) and C4 vegetation (~ -12 ‰). While in-stream CO_2 uptake during aquatic primary production and degassing of CO_2 along the river course make $\delta^{13}\text{C}_{\text{DIC}}$ less negative, the addition of respired CO_2 (with isotopic signature similar to the organic C substrate) and the increasing contribution of HCO_3^- (compared to CO_2) lowers the $\delta^{13}\text{C}_{\text{DIC}}$ (Finlay and Kendall, 2007). While carbon in HCO_3^- which originates from silicate rock weathering comes exclusively from CO_2 and will thus have a ^{13}C -depleted signature, carbonate weathering leads to more ^{13}C -enriched $\delta^{13}\text{C}_{\text{DIC}}$, since one half of the C in HCO_3^- is then derived from CaCO_3 and the other half from CO_2 .

The overall $\delta^{13}\text{C}_{\text{DIC}}$ values in all our samples ranged from -21.9 ‰ at the Zambezi source (during the 2013 dry season campaign) to -1.8 ‰ in the Kariba and the Cahora Bassa reservoirs (during the 2013 wet season), suggesting the occurrence of various C sources as well as in-stream processes. The overall average value of -7.3 ‰ and the good relationship between $\delta^{13}\text{C}_{\text{DIC}}$ and DSi : Ca^{2+} molar ratio, which explains 88 % of the variability in $\delta^{13}\text{C}_{\text{DIC}}$, point towards the influence of the relative importance of carbonate versus silicate mineral weathering (Fig. 7c). However, the increase in $\delta^{13}\text{C}_{\text{DIC}}$ along the Zambezi mainstem (Fig. 7d) along with an increase in POC in the lower Zambezi (data not shown), mostly laterally derived but also partially in-river produced (as suggested by increased primary production rates), points out the interplay between downstream degassing and the degradation of the organic matter in controlling $\delta^{13}\text{C}_{\text{DIC}}$ along the Zambezi River. A clear and instant effect of degassing with a fast increase in $\delta^{13}\text{C}$ of the remaining DIC pool explained by the ^{13}C depletion of the CO_2 fraction relative to HCO_3^- and CO_3^{2-} (Doctor et al., 2008) can be best seen at Victoria Falls, where during 2012 wet campaign we noticed a rapid increase in $\delta^{13}\text{C}_{\text{DIC}}$ from -8.5 to -6.9 ‰ (Fig. 7d) coinciding with a decrease in $p\text{CO}_2$ from 2500 to 640 ppm (Fig. 3a). Similar CO_2 degassing effects on $\delta^{13}\text{C}_{\text{DIC}}$ were also observed downstream of the Barotse Floodplain (ZBZ.5 to ZBZ.6, 195 km) and downstream of the Chobe Swamps (ZBZ.7 to ZBZ.8, 74 km), where, during the same 2012 wet campaign, the drop in $p\text{CO}_2$ from 7560 to 1890 ppm and 6307 to 2500 ppm, respectively, was accompanied by an increase in $\delta^{13}\text{C}_{\text{DIC}}$ from -8.5 to -6.9 ‰ and from -7.0 to -6.2 ‰, respec-

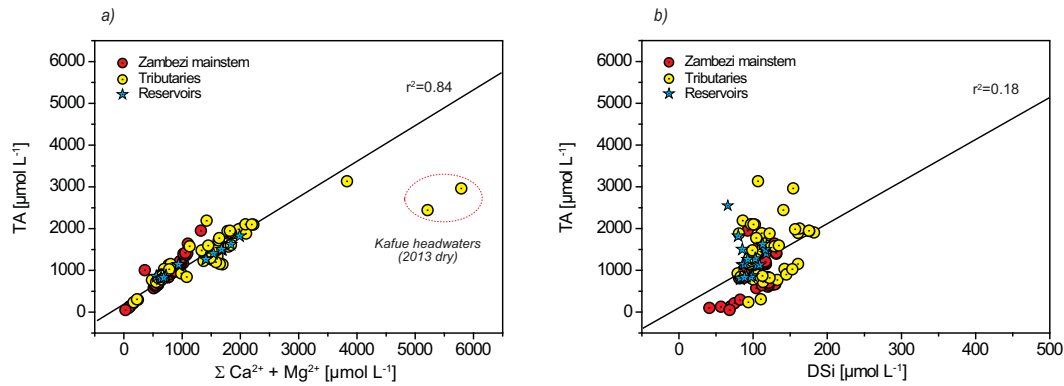


Figure 6. Relationships between the observed total alkalinity (TA) and (a) the sum of Ca^{2+} and Mg^{2+} , and (b) dissolved silica (DSi).

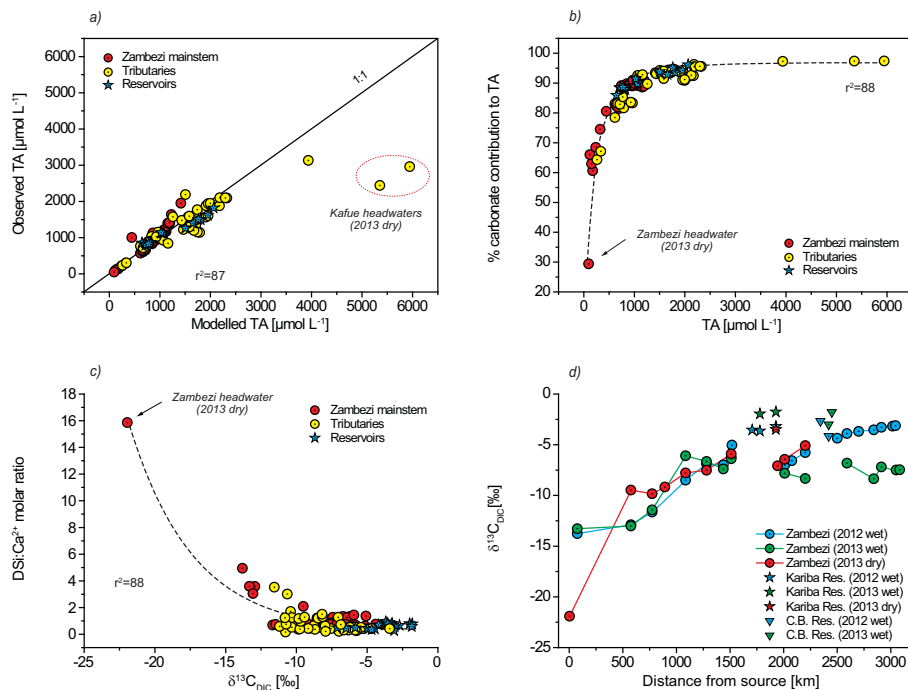


Figure 7. Relationships between (a) modeled and observed total alkalinity (TA), (b) the estimated contribution of TA derived from carbonate weathering to observed TA (see text for details), and (c) isotopic signature of DIC ($\delta^{13}\text{C}_{\text{DIC}}$) to $\text{DSi}:\text{Ca}^{2+}$ molar ratio. Panel (d) shows the spatiotemporal variability of $\delta^{13}\text{C}_{\text{DIC}}$ along the Zambezi mainstem.

tively (Figs. 3a, 7d). Ranging between -4.1 and -1.8‰ (mean -2.9‰), the $\delta^{13}\text{C}_{\text{DIC}}$ values in the surface waters of the Kariba and the Cahora Bassa reservoirs were highest among all samples during all three campaigns (Fig. 7d). Associated with mostly undersaturated CO_2 conditions and negative CO_2 fluxes (Figs. 3a, 9a), R rates (on the order of $\sim 0.8 \mu\text{mol CL}^{-1} \text{h}^{-1}$) not different than riverine values, and P rates ($\sim 25.0 \mu\text{mol CL}^{-1} \text{h}^{-1}$) half those of the river values, the higher $\delta^{13}\text{C}_{\text{DIC}}$ values found in both reservoirs on the Zambezi can be primarily explained by the atmospheric CO_2 uptake during primary production, a process capable of generating strong diel variations (Parker et al.,

2005). Slightly lower $\delta^{13}\text{C}_{\text{DIC}}$ values (-7.1 to -3.0‰ , mean -5.2‰) characterized the surface water of the Itezhi Tezhi Reservoir on the Kafue River. The observed $\delta^{13}\text{C}_{\text{DIC}}$ enrichment in the Itezhi Tezhi Reservoir with increasing distance from the river inflow correlated with a gradual decrease in $p\text{CO}_2$, and comparable R rates ($\sim 0.7 \mu\text{mol CL}^{-1} \text{h}^{-1}$) but higher P ($\sim 48.4 \mu\text{mol L}^{-1} \text{h}^{-1}$) suggest the combined effect of P and CO_2 evasion (mostly originating with river inflow). While $\delta^{13}\text{C}_{\text{DIC}}$ in the Kafue River ($-7.3 \pm 1.7\text{‰}$, $n = 26$, excluding the Itezhi Tezhi Reservoir) was not significantly different from that of the Zambezi mainstem ($-7.7 \pm 3.6\text{‰}$, $n = 42$, excluding the Kariba and the Cahora

Bassa reservoirs), $\delta^{13}\text{C}_{\text{DIC}}$ values of smaller tributaries were significantly lower. The $\delta^{13}\text{C}_{\text{DIC}}$ values of the Kabompo ($-10.7 \pm 0.7\text{‰}$, $n = 3$), Lunga ($-9.8 \pm 1.0\text{‰}$, $n = 5$), Lungwa ($-9.4 \pm 1.0\text{‰}$, $n = 8$), Lunsemfwa ($-8.9 \pm 1.7\text{‰}$, $n = 4$) and Mazoe tributaries (-9.4‰ , $n = 1$) would suggest that, in addition to carbonate weathering, there is a substantially increased contribution of soil CO_2 from C4 vegetation. Intermediate $\delta^{13}\text{C}_{\text{DIC}}$ values between reservoirs and tributaries were measured in the Shire River ($-5.1 \pm 2.4\text{‰}$, $n = 2$), which drains the soft-water Lake Malawi. These isotopically enriched $\delta^{13}\text{C}_{\text{DIC}}$ values there coupled with highest recorded $p\text{CO}_2$ concentrations (mean 13 350 ppm; Fig. 3d) must be explained by exceptionally high CO_2 degassing rates of over $23\,000\text{ mg C m}^{-2}\text{ d}^{-1}$, up to 1 order of magnitude larger than all other measured fluxes (Fig. 9a).

3.6 Diurnal variation in GHG concentrations

To account for the importance of diel fluctuations on the investigated biogeochemical parameters, we performed a 24 h sampling campaign at station ZBZ.11 on the Zambezi River between 22 and 23 November 2013 (dry season). Measurements show a small gradual increase in water temperature (of 0.7 °C) from midday to midnight follow by a decrease (of 0.6 °C) between midnight and 09:00 a.m., when temperature started rising again (Fig. 8a, b). Similar sinusoidal patterns were observed over the same time period for DO (increased saturation with 7%, decreased with 5% followed by increase), pH (increased from 6.95 to 7.32, decrease to 7.21 followed by increase), and $\delta^{13}\text{C}_{\text{DIC}}$ (increased from -6.4 to -5.5‰ , decrease to -6.1‰ followed by increase; Fig. 8c, d, e). In contrast, a reverse pattern was recorded for $p\text{CO}_2$, which gradually decreased by 30% (from 1655 to 1180 ppm) from midday to midnight ($\sim 40\text{ ppm h}^{-1}$) and increased by 30% (up to 1430 ppm) until 09:00 a.m. ($\sim 30\text{ ppm h}^{-1}$), when values start slowly decreasing with the onset of primary production (Fig. 8g). Following the $p\text{CO}_2$ pattern, DIC decreased 0.1 mmol L^{-1} (12%) between 09:00 and 12:00 a.m., and increased 0.03 mmol L^{-1} (3%) between 12:00 and 09:00 a.m. (Fig. 8f). While CH_4 followed the general pattern of $p\text{CO}_2$ (decreasing with $270\text{ }\mu\text{mol L}^{-1}$ and increasing with $150\text{ }\mu\text{mol L}^{-1}$ or $\sim 25\text{ }\mu\text{mol L}^{-1}\text{ h}^{-1}$), N_2O showed no distinct diurnal variations (Fig. 8h, i). While these patterns provide clear evidence of diel variations of physico-chemical parameters, likely caused by variations in the relative magnitude of P and R , their overall influence on the river biogeochemistry appears to be rather small. As, for obvious logistical reasons, we have sampled exclusively during daytime, the observed diel fluctuations suggest that, if anything, we may have possibly overestimated various parameters (i.e., dissolved gas concentrations and fluxes) by a maximum of 10 to 15%. To our knowledge, most existent studies which involved in situ measurements and data collection have been performed in the same manner, and are therefore subject to the same limitations.

3.7 CO_2 and CH_4 fluxes

The Zambezi River and all sampled tributaries were net sources of CO_2 and CH_4 to the atmosphere as a result of supersaturation in CO_2 and CH_4 with respect to atmospheric equilibrium (Figs. 3, 4). However, levels are well below the global emission range proposed by Aufdenkampe et al. (2011) and Bastviken et al. (2011) for tropical rivers and streams (Fig. 9a, b). Overall mean CO_2 and CH_4 fluxes of the Zambezi River of $3380\text{ mg C m}^{-2}\text{ d}^{-1}$ (median 1409) and $48.5\text{ mg C m}^{-2}\text{ d}^{-1}$ (median 12.4) were not different from those of the Kafue River of $3711\text{ mg C m}^{-2}\text{ d}^{-1}$ (median 1808) and $67.8\text{ mg C m}^{-2}\text{ d}^{-1}$ (median 14.7; Fig. 9). CO_2 fluxes along the Zambezi mainstem were generally lower during the 2013 dry season (mean $623\text{ mg C m}^{-2}\text{ d}^{-1}$) compared to fluxes of the 2012 and 2013 wet season campaigns (mean 3280 and $5138\text{ mg C m}^{-2}\text{ d}^{-1}$, respectively). The opposite situation was observed for CH_4 , where measured fluxes during 2013 wet campaign (no CH_4 fluxes were measured during the 2012 wet season; mean $26.5\text{ mg C m}^{-2}\text{ d}^{-1}$) were significantly lower compared to the 2013 dry season (mean $92.7\text{ mg C m}^{-2}\text{ d}^{-1}$). Singular events of negative CO_2 fluxes on the Zambezi mainstem were measured only during the 2013 dry season campaign at ZBZ.6 and ZBZ. 13 (mean -23 and $-33\text{ mg C m}^{-2}\text{ d}^{-1}$, respectively) and corresponded to riverine $p\text{CO}_2$ values of 300 and 421 ppm, respectively (Fig. 3a). A similar situation of undersaturated riverine CO_2 levels was also encountered on the Kafue River only during the 2013 dry season (at KAF.4, 330 ppm; Fig. 3b), but no reliable flux rate was determined there due to unusual, irregular fluctuations in CO_2 concentrations inside the floating chamber. With the exception of this, all other measured CO_2 fluxes on the Kafue River were positive, and fluxes of the 2013 dry season (mean $3338\text{ mg C m}^{-2}\text{ d}^{-1}$) were not significantly different from those of the two wet seasons (mean 2458 and $5355\text{ mg C m}^{-2}\text{ d}^{-1}$, respectively). As in the case of the Zambezi River, CH_4 fluxes along the Kafue were also higher during the 2013 dry season (mean $149.5\text{ mg C m}^{-2}\text{ d}^{-1}$) compared to the 2013 wet season (mean $16.8\text{ mg C m}^{-2}\text{ d}^{-1}$). Chamber measurements provide the combined CH_4 flux resulting from both ebullitive and diffusive fluxes. Since CH_4 concentrations during the dry season were not higher compared to the wet season (Fig. 4a, b), the most likely explanation for the higher CH_4 rates during low water levels observed along both Zambezi and Kafue rivers relates to higher contribution of ebullitive fluxes. This is consistent with higher CH_4 ebullitive fluxes during low waters than during high and falling waters in the Amazonian rivers (Sawakuchi et al., 2014). The higher contribution of CH_4 ebullition during the 2013 dry campaign is further supported by the comparison between total CH_4 flux (measured with the floating chamber) and the estimated diffusive CH_4 flux (F) from the interfacial mass transfer mechanism from water

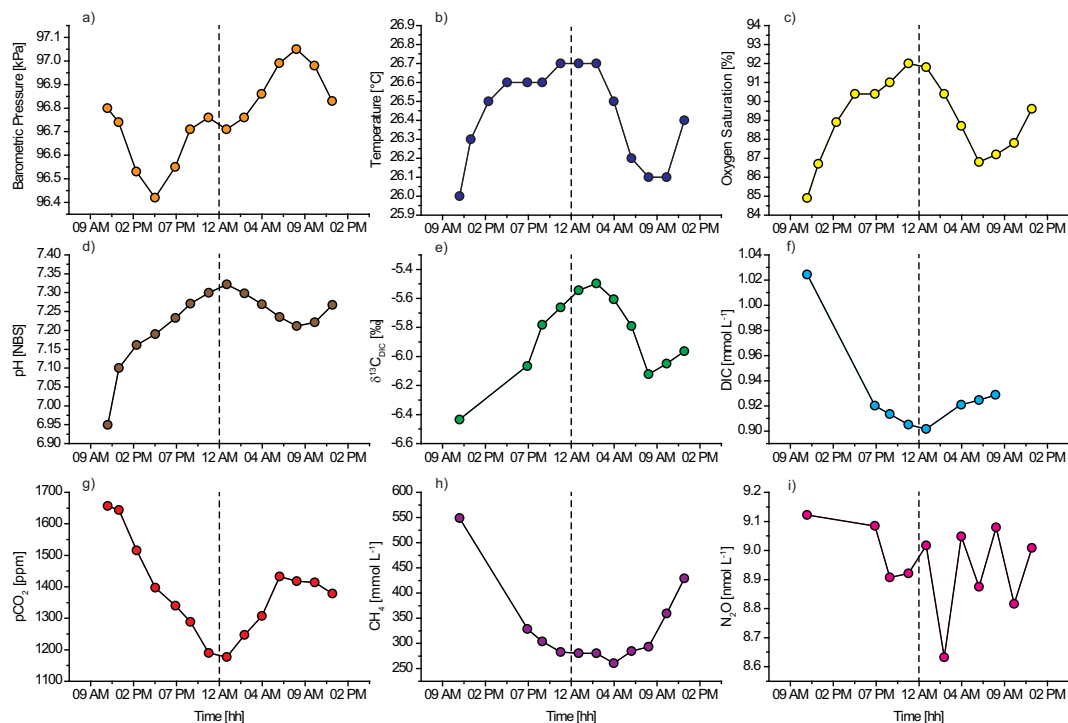


Figure 8. Diel variations of (a) barometric pressure, (b) temperature, (c) dissolved oxygen saturation (%DO), (d) pH, (e) isotopic signature of dissolved inorganic carbon ($\delta^{13}\text{C}_{\text{DIC}}$), (f) dissolved inorganic carbon concentrations (DIC), (g) partial pressure carbon dioxide ($p\text{CO}_2$), (h) methane (CH_4), and (i) nitrous oxide (N_2O) measured at ZBZ.11 between 22 and 23 November 2013.

to air, expressed as

$$F = k \cdot (C_w - C_{\text{eq}}), \quad (2)$$

where k is the gas transfer velocity back calculated from the measured CO_2 flux and normalized to a Schmidt number (Sc) of 600 ($k_{600} = k \times (600/Sc)^{-1/2}$), and C_w and C_{eq} are dissolved gas concentrations in the surface water and in the air, scaled by solubility to the value it would have when in equilibrium with the atmosphere. Assuming that the difference between the computed (diffusive) and measured CH_4 flux is purely due to ebullition, the comparison suggests that, on average, 73 % of measured CH_4 fluxes during the 2013 wet campaign along both the Zambezi and the Kafue rivers were due to diffusive processes and only 27 % originated from ebullition. In contrast, ebullition during the 2013 dry campaign accounted for up to 77 % of measured CH_4 fluxes. This is in agreement with the contribution of CH_4 ebullition of more than 50 % of total CH_4 emissions among different Amazonian rivers and seasons (Sawakuchi et al., 2014).

The k_{600} computed from CO_2 chamber flux measurements (on drift) ranged from 0.2 to 6.3 cm h^{-1} (mean 2.7, median 2.3 cm h^{-1}) for the Zambezi River, from 0.4 to 7.9 cm h^{-1} (mean 2.1, median 1.7 cm h^{-1}) for the Kafue River, and between 0.6 and 6.2 cm h^{-1} (mean 3.1, median 3.4 cm h^{-1}) for all other tributaries. These values are close to the k of $\sim 3 \text{ cm h}^{-1}$ suggested by Cole and Caraco (2001) for large

rivers but well below the median global values proposed by Aufdenkampe et al. (2011) for tropical rivers and streams (12.3 and 17.2 cm h^{-1} , respectively) and the basin-wide average value of 20.6 cm h^{-1} for the Zambezi given by Raymond et al. (2013). The higher value given by Raymond et al. (2013) corresponds to the average of the whole river network, including low-order streams that typically have high k values (Raymond et al., 2012), while our data were obtained mainly in high-order tributaries and mainstem. A few extreme k values (20.3 to 79.7 cm h^{-1}) obtained from the flux chamber measurements performed in static mode (non-drift) and explained by additional induced turbulence by the water rushing against the chamber walls have been excluded from the overall calculations. In situ experiments, mostly on the Congo River, designed to explore the effect of additionally induced turbulence by the chamber walls on the flux chamber determination in rivers, and performed both in static mode at various water velocities and drift mode, suggest a clear, linear dependency of k on the velocity of water relative to the floating chamber (Cristian R. Teodoru, unpublished data).

It is worth noting that the highest CO_2 fluxes along both Zambezi and Kafue rivers were found mostly in or downstream of wetlands and floodplains (i.e., $\sim 12\,500 \text{ mg C m}^{-2} \text{ d}^{-1}$, downstream of the Barotse Floodplain; $> 4000 \text{ mg C m}^{-2} \text{ d}^{-1}$ downstream of the Chobe Swamps; $> 12\,700 \text{ mg C m}^{-2} \text{ d}^{-1}$ in and downstream of the

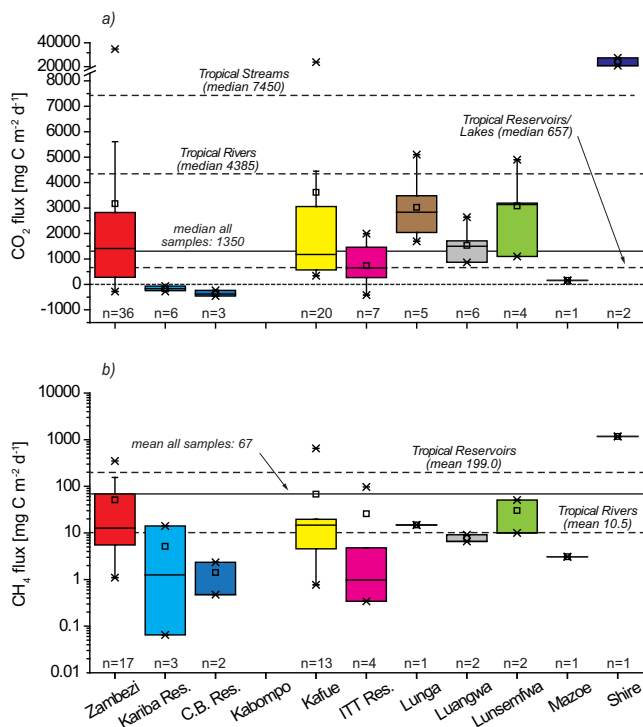


Figure 9. Measured range in (a) CO₂ fluxes and (b) CH₄ fluxes (note the log scale in the latter) for the Zambezi mainstem, tributaries and reservoirs. Box plots show the range, percentile, median, mean and outliers. Dashed lines in (a) represent global median CO₂ efflux for tropical rivers, streams and lakes/reservoirs based on Aufdenkampe et al. (2011), while in (b) they represent the global mean CH₄ emission for tropical rivers and reservoirs as suggested by Bastviken et al. (2011). Solid lines represent median CO₂ emissions (a) and mean CH₄ flux (b) of all sites and over the entire sampling period.

Kafue Flats) and in the delta ($> 10\,000\text{ mg C m}^{-2}\text{ d}^{-1}$). Such high outgassing rates there are consistent with findings of studies on the Amazonian river–floodplains system which stress the importance of wetlands and floodplains on river biogeochemistry, especially on the CO₂ fluxes (Richey et al., 2002; Abril et al., 2014). Moreover, the highest CO₂ and CH₄ fluxes of the Zambezi mainstem ($> 20\,000$ and $154\text{ mg C m}^{-2}\text{ d}^{-1}$, respectively) were consistently measured at ZBZ.18 immediately downstream of the confluence with the Shire River. The only outlet of Lake Malawi, the Shire River, passes through a large stagnant water complex of swamp/mashes (the Elephant Marsh) before it joins the Zambezi River. With mean CO₂ and CH₄ fluxes in the region of $23\,100$ and $1170\text{ mg C m}^{-2}\text{ d}^{-1}$, respectively, and much higher than the global emission level for tropical streams (Fig. 9), the Shire River represents a hotspot for both CO₂ and CH₄ emissions. Average CO₂ and CH₄ emissions for all tributaries (excluding the Kafue River) of 4790 (median 2641) and $180.7\text{ mg C m}^{-2}\text{ d}^{-1}$ (median 10.1), respectively, while higher than of the Zambezi mainstem, are still well be-

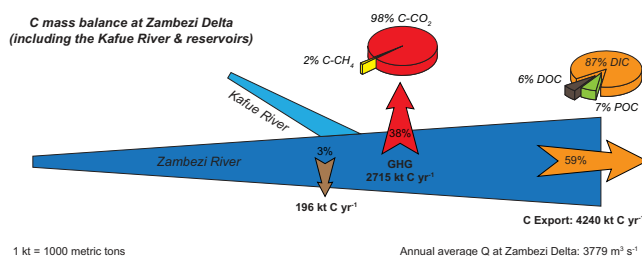


Figure 10. Carbon mass budget for the Zambezi River. The GHG emission component was calculated for a total surface area of $10\,576\text{ km}^2$, of which the Zambezi mainstem represents 18 %, the Kafue River accounts for 3 %, the Itzhi Tezhi and Kafue Gorge reservoirs sum up to approximately 4 %, and the Kariba and Cahora Bassa reservoirs represent 75 % (see Table 1).

low the global level for tropical rivers and streams (Fig. 9). In contrast, the two reservoirs on the Zambezi rivers (the Kariba and the Cahora Bassa) were both sinks of atmospheric CO₂ (mean -141 and $-356\text{ mg C m}^{-2}\text{ d}^{-1}$) but small sources of CH₄ (5.2 and $1.4\text{ mg C m}^{-2}\text{ d}^{-1}$, respectively; Fig. 9). A different situation was encountered for the much smaller Itzhi Tezhi Reservoir on the Kafue River, where average CO₂ emission in the range of $737\text{ mg C m}^{-2}\text{ d}^{-1}$ (median 644) approaches the global emission rate for tropical lakes and reservoirs (Fig. 9a), but the CH₄ flux of $25.8\text{ mg C m}^{-2}\text{ d}^{-1}$ is still below the reported global range (Fig. 9b).

Using the GWP (global warming potential) factor of CH₄ of 34 CO₂ equivalent (CO₂eq) for a 100-year time horizon (IPCC, 2013), mean CH₄ fluxes of the Zambezi and Kafue rivers' mainstem would translate into 1650 and $2305\text{ mg C-CO}_2\text{eq m}^{-2}\text{ d}^{-1}$, respectively, slightly lower but comparable with the magnitude of CO₂ fluxes (3380 and $3711\text{ mg C m}^{-2}\text{ d}^{-1}$, respectively). However, CH₄ emissions from tributaries (without Kafue) and reservoirs of 6145 and $460\text{ mg C-CO}_2\text{eq m}^{-2}\text{ d}^{-1}$, respectively, are distinctly higher, surpassing the equivalent CO₂ emissions by 1.5- and 2-fold, respectively.

Victoria Falls on the upper Zambezi forms another important hotspot for GHG emissions. A simple calculation suggests that the instant and almost complete degassing of CO₂ (75 %) and CH₄ (97 %) during the 2013 wet season campaign as the water dropped over the 108 m depth of the falls at a rate of $1245\text{ m}^3\text{ s}^{-1}$ released approximately 75 t C d^{-1} as CO₂ and 0.4 t C d^{-1} as CH₄. For CO₂, this is equivalent to what the Zambezi River would emit over an area of more than 20 km^2 or over a stretch of 33 km length for an average river width of 600 m .

3.8 C mass balance

We constructed a simple C mass balance over the study period for the Zambezi River which consists of three main components: (i) the outgassed load to the atmosphere, (ii) the C load to the sediment, and (iii) the C export load to the ocean

(Fig. 10). The GHG load to the atmosphere was calculated as the product between surface area and the measured areal CO_2 and CH_4 fluxes. The surface area of rivers was estimated by mapping each river sector between two sampling points using the geometrical applications in Google Earth Pro. Each sector was then multiplied by the corresponding average flux of the two bordering sampling points and results were summed up to calculate the overall GHG load (in kt C yr^{-1}). Estimates of river surface area were restricted to the Zambezi mainstem (1879 km^2 without reservoirs) and the Kafue River (287 km^2 without reservoirs; Table 1a), for which we have a relatively good longitudinal distribution of data, and where an extrapolation between sampling stations can be made with some confidence. Back-calculated from the overall riverine CO_2 and CH_4 loads to the atmosphere divided by total river surface, area weighted-average fluxes for the Zambezi River (4291 and $45.0 \text{ mg C m}^{-2} \text{ d}^{-1}$, respectively) and the Kafue River (2962 and $20.0 \text{ mg C m}^{-2} \text{ d}^{-1}$, respectively; Table 1a) are higher for the Zambezi and lower for the Kafue than corresponding arithmetic average fluxes. In the absence of reliable areal estimates for the rest of hydrological network, fluxes of all other sampled tributaries, even potentially important, were not included in the overall emission calculation. GHG emissions for reservoirs were calculated as a product between the corresponding mean fluxes and surface area (Table 1a). The surface area of the Kariba (5364 km^2), Cahora Bassa (2670 km^2), Itezhi Tezhi (364 km^2) and Kafue Gorge (13 km^2) reservoirs were taken from the literature (Beilfuss and dos Santos, 2001; Kunz et al., 2011a, b; Kling et al., 2014). CO_2 and CH_4 emissions for the Kafue Gorge Reservoir were extrapolated using mean fluxes of the Itezhi Tezhi Reservoir.

C deposition was estimated considering only removal in reservoirs, while deposition in rivers, in the absence of direct measurements, was assumed negligible. C deposition in the Kariba and the Itezhi Tezhi reservoirs of 120 and 16 kt C yr^{-1} , respectively, was taken from available literature data (Kunz et al., 2011a, b), while C retention in the Cahora Bassa and the Kafue Gorge reservoirs of 60 and 0.6 kt C yr^{-1} , respectively, was extrapolated from the rates of the Kariba and the Itezhi Tezhi reservoirs (Table 1a).

The export load to the ocean (Table 1b) was computed as the product between the annual flow rate (Q) and the average POC (2.6 mg L^{-1}), DOC (2.2 mg L^{-1}) (own unpublished data) and DIC (30.8 mg L^{-1}) measured at the two stations in the delta, close to the river mouth (ZBZ.19 and ZBZ.20). Due to a lack of direct discharge measurements at the river mouth over the study period, an annual average flow rate of $3779 \text{ m}^3 \text{ s}^{-1}$ was calculated from the existing literature data of 3424 and $4134 \text{ m}^3 \text{ s}^{-1}$ (Beilfuss and dos Santos, 2001; World Bank, 2010).

Mass balance calculations suggest a total C yield of 7215 kt yr^{-1} (or $5.2 \text{ t C km}^{-2} \text{ yr}^{-1}$), of which (i) 38 % ($2779 \text{ kt C yr}^{-1}$) is annually emitted into the atmosphere, mostly in the form of CO_2 (98 %); (ii) 3 % (196 kt C yr^{-1})

is removed by sedimentation in the main reservoirs; and (iii) 59 % ($4240 \text{ kt C yr}^{-1}$) is exported to the ocean, mostly in the form of DIC (87 %), with organic C component accounting only for a small fraction (7 % POC and 6 % DOC; Fig. 10). Even potentially large uncertainties for the overall balance may occur from the lack of direct discharge measurements at the river mouth, the limitation of riverine GHG emission only to the mainstem of the Zambezi and the Kafue rivers, and from missing data on C removal by sedimentation in rivers, the overall picture is rather consistent with previous figures of global C budgets (Cole et al., 2007; Battin et al., 2009). It is worth mentioning that our relatively lower C emissions component of the balance compared to global budgets is the direct result of atmospheric CO_2 uptake by the surface waters of the Kariba and Cahora Bassa reservoirs (Table 1). Despite their relatively low uptake rates (-141 and $-356 \text{ mg C m}^{-2} \text{ d}^{-1}$, respectively; Table 1), the huge areal extent of the two reservoirs, which accounts for more than 76 % of the total estimated aquatic surface used in the budget, lowered the overall outgassed load by 20 %. This in turn reduces the relative contribution of the C emission component of the balance by 6 %. In other words, if both reservoirs on the Zambezi were C-neutral (most likely situation since the atmospheric CO_2 uptake must be compensated for by rapid release of hypolimnetic CO_2 pool with the disruption of thermal stratification during the winter period in July–August), the relative contribution of emissions, deposition and export to the total budget would reach 43, 3 and 54 %, respectively. The influence of reservoirs on riverine C budget can be clearly seen in the case of Kafue River, where a similar balance approach would suggest a reverse situation with emissions surpassing the downstream export by almost 2-fold. With both Itezhi Tezhi and Kafue Gorge reservoirs contributing one-third to the total emissions of 417 kt C yr^{-1} (Table 1a), a C burial rate of 17 kt C yr^{-1} (Table 1a) and an export load of around 258 kt C yr^{-1} , this would translate into a similar C yield of $4.4 \text{ t C km}^{-2} \text{ yr}^{-1}$ (691 kt yr^{-1}), but the balance between emission, deposition and export components would be shifted to 60, 3 and 37 %, respectively.

Failing to incorporate C emissions from the entire hydrological network of the Zambezi River basin clearly underestimates the overall C outgassing load. For instance, using a total river and stream area of 7325 km^2 for the Zambezi Basin (excluding lakes and reservoirs) derived from a limnity index of 0.42 % and a total catchment area of $1\,730\,000 \text{ km}^2$ (Raymond et al., 2013), as well as a mean CO_2 and CH_4 flux of 3630 and $32.5 \text{ mg C m}^{-2} \text{ d}^{-1}$, respectively (average between Zambezi and Kafue values, Table 1a), GHG emission from the entire Zambezi River network would reach $\sim 9780 \text{ kt C yr}^{-1}$. Taking further into account C emissions and sinks in reservoirs and the export load to the ocean, a simple calculation would suggest a total C yield of $\sim 13\,710 \text{ kt yr}^{-1}$ ($\sim 10 \text{ t C km}^{-2} \text{ yr}^{-1}$), of which GHG emissions account for up to 68 %, while the export load represent less than 30 %. Moreover, the relative contribution

Table 1. (a) Carbon emission estimates based on measured CO₂ and CH₄ fluxes (this work) and carbon removal by deposition in reservoirs based on available published data (Kunz et al., 2011a, b); (b) carbon export loads to the ocean calculated using average literature river discharge at the Zambezi Delta and POC, DOC and DIC concentrations (this work) measured at the river mouth (ZBZ.19 and ZBZ.20) during the 2012 and 2013 wet season campaigns; and (c) carbon mass balance components including yield, emission, deposition and export. Data marked with * represent areal fluxes recalculated for the entire surface including reservoirs. Carbon deposition in the Kafue Gorge and Cahora Bassa reservoirs (***) were estimated assuming same deposition rates of the Itzhi Tezhi and the Kariba reservoirs. All loads are expressed in kt C yr⁻¹.

(a)							
River/reservoir	Area [km ²]	CO ₂ flux [mg C m ⁻² d ⁻¹]	CH ₄ flux	CO ₂	CH ₄	Emission [kt C yr ⁻¹]	Deposition
Kafue River without reservoirs	287	2962	20.0	310	2.1	312	–
Itzhi Tezhi Reservoir	364	737	25.8	98	3.4	101	16
Kafue Gorge Reservoir	13	737	25.8	3	0.1	4	1**
Kafue River with reservoirs	664	1698*	23.3*	411	5.6	417	17
Zambezi River without reservoirs	1879	4291	45.0	2943	30.8	2974	–
Kariba Reservoir	5364	–141	5.2	–276	10.1	–266	120
Cahora Bassa Reservoir	2670	–356	1.4	–347	1.4	–346	60**
Zambezi River with reservoirs	9913	641*	11.7*	2319	42.3	2362	180
Zambezi and Kafue rivers with reservoirs	10 576	707*	12.4*	2731	48.0	2779	196
(b)							
River	Q [m ³ s ⁻¹]	POC	DOC [mg L ⁻¹]	DIC	POC	DOC [kt C yr ⁻¹]	DIC
Zambezi River at delta	3779	2.6	2.2	30.8	306	263	3672
(c)							
	Yield	Emission	Deposition	Export	Emission	Deposition	Export
		[kt C yr ⁻¹]				[%]	
Carbon balance at Zambezi Delta	7215	2779	196	4240	38	3	59

of GHG to the present C budget would increase considerably if taking into account emissions from the highly productive systems such as wetlands and floodplains, of which influence on the biogeochemistry of the river has been clearly demonstrated throughout this work and elsewhere (Aufdenkampe et al., 2011; Abril et al., 2014). For instance, a rough estimate of C emissions from the only four major floodplain/wetlands in the basin (the Barotse Floodplain: 7700 km²; the Chobe Swamps: 1500 km²; the Lukanga Swamps: 2100 km²; and the Kafue Flats: 6500 km²) calculated using our fluxes measured on the river downstream of their locations, and applied to merely half of their reported surface area and over only the seasonal flooding period (half-year), would add an extra 16 000 kt C yr⁻¹ to the overall emissions. Assuming no further C deposition in these areas, the incorporation of wetlands into the present budget would increase the total C yield to 17 t C km⁻² yr⁻¹ (or 23 400 kt C yr⁻¹), while the relative contribution of degassing would reach 81 % (19 000 kt C yr⁻¹). While the flux term of our budget may represent a low-limit estimate, further research and more quantitative data are needed in order to improve our understanding of the links between river and wetlands and to better

constrain the role of aquatic systems as a whole in both regional and global C budgets.

4 Concluding remarks

Overall, results of this catchment-scale study demonstrate that riverine GHGs, despite their interannual and seasonal variations, appeared to be mainly controlled by the connectivity with floodplains/wetlands, the presence of rapids/waterfalls and the existence of large man-made structures along the aquatic continuum. While TA, $\delta^{13}\text{C}_{\text{DIC}}$ and DSi:Ca²⁺ values suggest the importance of both carbonate weathering and in-stream processes in controlling riverine DIC, the covariation of $p\text{CO}_2$ with CH₄ suggests that both dissolved gases in this river system are largely controlled by organic matter degradation processes. While comparable with other studied river systems in Africa, the range in GHG concentrations and fluxes in the Zambezi River basin were generally below the reported global median for tropical rivers, streams and lakes/reservoirs, for which the current empirical data set is strongly biased towards studies of the Amazon River basin. While GHG concentrations and eva-

sion rates may generally be higher in the Amazon Basin, up-scaling from that region to the whole tropical zone is prone to high uncertainties. Our C mass balance for the Zambezi River suggest that GHG emission to the atmosphere represents less than 40 % of the total budget, with C export to the ocean (mostly as DIC) being the dominant component (59 %). However, the importance of GHG emissions in the overall budget is likely underestimated since our analyses do not take into account fluxes from the entire hydrological network (i.e., all tributaries), and since potentially large emissions that occur in the seasonally flooded wetlands and floodplains have not been estimated.

The Supplement related to this article is available online at doi:10.5194/bg-12-2431-2015-supplement.

Acknowledgements. Funding for this work was provided by the European Research Council (ERC-StG240002, AFRIVAL – African river basins: catchment-scale carbon fluxes and transformations, <http://ees.kuleuven.be/project/afriaval/>) and the Research Foundation Flanders (FWO-Vlaanderen, travel grants K2.011.12N and K2.266.13N to Cristian R. Teodoru). Alberto V. Borges is a senior research associate at the FRS-FNRS. We thank Zita Kelemen (KU Leuven) for technical and laboratory assistance; Marc-Vincent Commarieu (University of Liège) for the TA measurements; Kristin Coorevits and Stijn Baeken (KU Leuven) for ICP-MS measurements; Peter Salaets (KU Leuven) for nutrient analyses; and Stephan Hoornaert and Sandro Petrovic (University of Liège), who carried out part of the CH₄ measurements. We thank all the generous and helpful people (Maurice Diamond, Sam Talbot, Tony Weber, Ann-Marie Butzelaar, Andrew Peter Dekker, and many others) for logistical support during sampling. The three anonymous reviewers provided useful comments and suggestions that allowed us to improve the previous version of the manuscript.

Edited by: T. J. Battin

References

- Abril, G., Martinez, J. M., Artigas, L. F., Moreira-Turcq, P., Benedetti, M. F., Vidal, L., Meziane, T., Kin, J. H., Bernardes, M. C., Savoye, N., Deborde, J., Souza, E. L., Albéric, P., Landim de Souza, M. F., and Roland, F.: Amazon River carbon dioxide outgassing fuelled by wetlands, *Nature*, 505, 395–398, doi:10.1038/nature12797, 2014.
- Abril, G., Bouillon, S., Darchambeau, F., Teodoru, C. R., Marwick, T. R., Tamooh, F., Ochieng Omengo, F., Geeraert, N., Deirmendjian, L., Polsenaere, P., and Borges, A. V.: Technical Note: Large overestimation of pCO₂ calculated from pH and alkalinity in acidic, organic-rich freshwaters, *Biogeosciences*, 12, 67–78, doi:10.5194/bg-12-67-2015, 2015.
- Amiotte-Suchet, P., Aubert, D., Probst, J. L., Gauthier-Lafaye, F., Probst, A., Andreux, F., and Viville, D.: $\delta^{13}\text{C}$ pattern of dissolved inorganic carbon in a small granitic catchment: the Strengbach case study (Vosges mountains, France), *Chem. Geol.*, 159, 129–145, 1999.
- Ashton, P. J., Love, D., Mahachi, H., and Dirks, P. H. G. M.: An overview of the impact of mining and mineral processing operations on water resources and water quality in the Zambezi, Limpopo and Olifants Catchments in Southern Africa., Contract Report to the Mining, Minerals and Sustainable Development (SOUTHERN AFRICA), Project by CSIR-Environmentek, Pretoria, South Africa and Geology Department, University of Zimbabwe, Harare, Zimbabwe, Rep. ENV-P-C 2001–042, 336 pp., available at: <http://pubs.iied.org/pdfs/G00599.pdf> (last access: 15 September 2014), 2001.
- Aufdenkampe, E. K., Mayorga, E., Raymond, P. A., Melack, J. M., Doney, S. C., Alin, S. R., Aalto, R. E., and Yoo, K.: Rivers key to coupling biogeochemical cycles between land, oceans and atmosphere, *Front. Ecol. Environ.* 9, 53–60, doi:10.1890/100014, 2011.
- Bastviken, D., Tranvik, L. J., Downing, J. A., Crill, P. M., and Enrich-Prast, A.: Freshwater methane emissions offset the continental carbon sink, *Science*, 331, 6013, 50, doi:10.1126/science.1196808, 2011.
- Battin, T. J., Luysaert, S., Kaplan, L. A., Aufdenkampe, A. K., Richter, A., and Tranvik, L. J.: The boundless carbon cycle, *Nat. Geosci.*, 2, 598–600, doi:10.1038/ngeo618, 2009.
- Beilfuss, R. and dos Santos, D.: Patterns of hydrological change in the Zambezi Delta, Mozambique, Working Paper #2: Program for the sustainable management of Cahora Bassa Dam and the Lower Zambezi Valley, USA, International Crane Foundation, Direcção Nacional de Aguas, Mozambique, 2001.
- Berggren, M., Lapierre, J.-F., and del Giorgio, P. A.: Magnitude and regulation of bacterioplankton respiratory quotient across freshwater environmental gradients, *ISME J.*, 6, 984–993, doi:10.1038/ismej.2011.157, 2012.
- Bouillon, S., Abril, G., Borges, A. V., Dehairs, F., Govers, G., Hughes, H. J., Merckx, R., Meysman, F. J. R., Nyunja, J., Osburn, C., and Middelburg, J. J.: Distribution, origin and cycling of carbon in the Tana River (Kenya): a dry season basin-scale survey from headwaters to the delta, *Biogeosciences*, 6, 2475–2493, doi:10.5194/bg-6-2475-2009, 2009.
- Bouillon, S., Yambélé, A., Spencer, R. G. M., Gillikin, D. P., Hernes, P. J., Six, J., Merckx, R., and Borges, A. V.: Organic matter sources, fluxes and greenhouse gas exchange in the Oubangui River (Congo River basin), *Biogeosciences*, 9, 2045–2062, doi:10.5194/bg-9-2045-2012, 2012.
- Bouillon, S., Yambélé, A., Gillikin, D. P., Teodoru, C. R., Darchambeau, F., Lambert, T., and Borges, A. V.: Contrasting biogeochemical characteristics of the Oubangui River and tributaries (Congo River basin), *Sci. Rep.*, 4, 1–10, doi:10.1038/srep05402, 2014.
- Briggs, D. A. and Mitchell, C. J.: Mineralogy and beneficiation of some industrial minerals from Zambia, *Zamb. J. Appl. Earth Sci.*, 5, 18–27, 1991.
- Butman, D. and Raymond, P. A.: Significant efflux of carbon dioxide from streams and rivers in the United States, *Nat. Geosci.*, 4, 839–842, doi:10.1038/ngeo1294, 2011.
- Cole, J. J. and Caraco, N. F.: Carbon in catchments: connecting terrestrial carbon losses with aquatic metabolism, *Mar. Freshwater Res.*, 52, 101–110, 2001.

- Cole, J. J., Prairie, Y. T., Caraco, N. F., McDowell, W. H., Tranvik, L. J., Striegl, R. G., Duarte, C. M., Kortelainen, P., Downing, J. A., Middelburg, J. J., and Melack, J.: Plumbing the global carbon cycle: integrating inland waters into the terrestrial carbon budget, *Ecosystems*, 10, 171–184, 2007.
- Chenje, M.: State of the Environment Zambezi Basin 2000, SADC, IUCN, ZRA, and SARDC, Maseru, Lusaka and Harare, 334 pp., ISBN 978-1-77910-009-2, 2000.
- Dauchez, S., Legendre, L., and Fortier, L.: Assessment of simultaneous uptake of nitrogenous nutrients (^{15}N) and inorganic carbon (^{13}C) by natural phytoplankton populations, *Mar. Biol.*, 123, 651–666, 1995.
- Doctor, D. H., Kendall, C., Sebestyen, S. D., Shanley, J. B., Ohte, N., and Boyer, E. W.: Carbon isotope fractionation of dissolved inorganic carbon (DIC) due to outgassing of carbon dioxide from a headwater stream, *Hydrol. Process.*, 22, 2410–2423, 2008.
- Driscoll, C. T., Fuller, R. D., and Schecher, W. D.: The role of organic acids in the acidification of surface waters in the eastern US, *Water Air Soil Poll.*, 43, 21–40, 1989.
- Einola, E., Rantakari, M., Kankaala, P., Kortelainen, P., Ojala, A., Pajunen, H., Mäkelä, S., and Arvola, L.: Carbon pools and fluxes in a chain of five boreal lakes: a dry and wet year comparison, *J. Geophys. Res.*, 116, G03009, doi:10.1029/2010JG001636, 2011.
- Finlay, J. C.: Controls of streamwater dissolved inorganic carbon dynamics in a forested watershed, *Biogeochemistry*, 62, 231–252, doi:10.1023/A:1021183023963, 2003.
- Finlay, J. C. and Kendall, C.: Stable isotope tracing of temporal and spatial variability in organic matter sources to freshwater ecosystems, in: *Stable Isotopes in Ecology and Environmental Science*, 2nd edn., edited by: Michener, R. and Lajtha, K., Blackwell Publishing, Oxford, UK, 283–333, 2007.
- Garrels, R. M. and Mackenzie, F. T.: *Evolution of Sedimentary Rocks*, W. W. Norton, New York, 397 pp., 1971.
- Gillikin, D. P. and Bouillon, S.: Determination of $\delta^{18}\text{O}$ of water and $\delta^{13}\text{C}$ of dissolved inorganic carbon using a simple modification of an elemental analyzer – isotope ratio mass spectrometer (EA-IRMS): an evaluation, *Rapid Commun. Mass Sp.*, 21, 1475–1478, 2007.
- Guasch, H., Armengol, J., Martí, E., and Sabater, S.: Diurnal variation in dissolved oxygen and carbon dioxide in two low-order streams, *Water Res.*, 32, 1067–1074, doi:10.1016/S0043-1354(97)00330-8, 1998.
- Guérin, F., Abril, G., Richard, S., Burban, B., Reynouard, C., Seyler, P., and Delmas, R.: Methane and carbon dioxide emissions from tropical reservoirs: significance of downstream rivers. *Geophys. Res. Lett.*, 33, L21407, doi:10.1029/2006GL027929, 2006.
- Hemold, H. F.: Acid neutralizing capacity, alkalinity, and acid-base status of natural waters containing organic acids, *Environ. Sci. Technol.*, 24, 1486–1489, 1990.
- Hunt, C. W., Salisbury, J. E., and Vandemark, D.: Contribution of non-carbonate anions to total alkalinity and overestimation of pCO_2 in New England and New Brunswick rivers, *Biogeochemistry*, 8, 3069–3076, doi:10.5194/bg-8-3069-2011, 2011.
- IPCC: Working group I contribution to the fifth assessment report (AR5) of the intergovernmental panel on climate change, in: *Climate Change 2013: The Physical Science Basis*, Cambridge University Press, Cambridge, United Kingdom and New York, NY, USA, 1552 pp., 2013.
- Kling, G. W., Kipphut, G. W., and Miller, M. C.: Arctic lakes and streams as gas conduits to the atmosphere: implications for tundra carbon budgets, *Science*, 251, 298–301, doi:10.1126/science.251.4991.298, 1991.
- Kling, H., Stanzel, P., and Preishuber, M.: Impact modelling of water resources development and climate scenarios on Zambezi River discharge, *J. Hydrol. Reg. Stud.*, 1, 17–43 2014.
- Koné, Y. J. M., Abril, G., Kouadio, K. N., Delille, B., and Borges, A. V.: Seasonal variability of carbon dioxide in the rivers and lagoons of Ivory Coast (West Africa), *Estuar. Coast.*, 32, 246–260, 2009.
- Koné, Y. J. M., Abril, G., Delille, B., and Borges, A. V.: Seasonal variability of methane in the rivers and lagoons of Ivory Coast (West Africa), *Biogeochemistry*, 100, 21–37, 2010.
- Kunz, M. J., Anselmetti, F. S., Wuestm, A., Wehrli, B., Vollenweider, A., Thuring, S., and Senn, D. B.: Sediment accumulation and carbon, nitrogen, and phosphorus deposition in the large tropical reservoir Lake Kariba (Zambia/Zimbabwe), *J. Geophys. Res.*, 116, G03003, doi:10.1029/2010JG001538, 2011a.
- Kunz, M. J., Wuest, A., Wehrli, B., Landert, J., and Senn, D. B.: Impact of a large tropical reservoir on riverine transport of sediment, carbon and nutrients to downstream wetlands, *Water Resour. Res.*, 47, W12531, doi:10.1029/2011WR010996, 2011b.
- Kunz, M. J., Senn, D. B., Wehrli, B., Mwelwa, E. M., and Wüest, A.: Optimizing turbine withdrawal from a tropical reservoir for improved water quality in downstream wetlands. *Water Resour. Res.*, 49, 1–15, doi:10.1002/wrcr.20358, 2013.
- Lambert, T., Darchambeau, F., Bouillon, S., Alhou, B., Mbega, J - D, Teodoru, C. R., Nyoni, F. C., and A V Borges, A. V.: The effect of vegetation cover on the spatial and temporal variability of dissolved organic carbon and chromophoric dissolved organic matter in large African rivers, submitted, 2015.
- Lewis, E. and Wallace, D. W. R.: Program developed for CO_2 system calculations, ORNL/CDIAC-105, published by Carbon Dioxide Information Analysis Center, Oak Ridge National Laboratory, U.S. Department of Energy, Oak Ridge, Tennessee, 1998.
- Ludwig, W., Probst, J.-L., and Kempe, S.: Predicting the oceanic input of organic carbon by continental erosion, *Global Biogeochem. Cy.*, 10, 23–41, 1996.
- Mann, P. J., Spencer, E. G. M., Dinga, B. J., Poulsen, J. R., Hernes, P. J., Fiske, G., Salter, M. E., Wang, Z. A., Hoering, K. A., Six, J., and Holmes, R. M.: The biogeochemistry of carbon across a gradient of streams and rivers within the Congo Basin, *J. Geophys. Res.-Biogeo.*, 119, 687–702, 2014.
- Marwick, T. R., Tamooh, F., Ogwoka, B., Teodoru, C., Borges, A. V., Darchambeau, F., and Bouillon, S.: Dynamic seasonal nitrogen cycling in response to anthropogenic N loading in a tropical catchment, Athi-Galana-Sabaki River, Kenya, *Biogeosciences*, 11, 443–460, doi:10.5194/bg-11-443-2014, 2014.
- McCartney, M. P. and Houghton-Carr, H. A.: Modelling approach to assess inter-sectoral competition for water resources in the Kafue Flats, Zambia, *Water Environ. J.*, 12, 101–106, doi:10.1111/j.1747-6593.1998.tb00157.x, 1998.
- McCartney, M., Cai, X., and Smakhtin, V.: Evaluating the flow regulating functions of natural ecosystems in the Zambezi River Basin, *IWMI Res. Rep. 148*, International Water Management Institute (IWMI), Colombo, Sri Lanka, 59 pp., doi:10.5337/2013.206, 2013.

- Mengis, M. R., Gächter, R., and Wehrli, B.: Sources and sinks of nitrous oxide (N₂O) in deep lakes, *Biogeochemistry*, 38, 281–301, 1997.
- Meybeck, M.: Global chemical-weathering of surficial rocks estimated from river dissolved loads, *Am. J. Sci.*, 287, 401–428, 1987.
- Millero, F. J.: The thermodynamics of the carbonic acid system in seawater, *Geochim. Cosmochim. Ac.*, 43, 1651–1661, 1979.
- Moore, A. E., Cotterill, F. P. D., Main, M. P. L., and Williams, H. B.: The Zambezi River, in: *Large Rivers: Geomorphology and Management*, edited by: Gupta, A., John Wiley & Sons, Ltd, Chichester, UK, 311–333, 2007.
- Mook, W. G., Koopmans, M., Carter, A. F., and Keeling, C. D.: Seasonal, latitudinal, and secular variations in the abundance and isotopic ratios of atmospheric carbon dioxide: 1. Results from land stations, *J. Geophys. Res.*, 88, 10915–10933, 1983.
- Mumba, M. and Thompson, J. R.: Hydrological and ecological impacts of dams on the Kafue Flats floodplain system, southern Zambia, *Phys. Chem. Earth*, 30, 442–447, 2005.
- Parker, S. R., Poulson, S. R., Gammons, C. H., and Degrandpre, M. D.: Biogeochemical controls on diel cycling of stable isotopes of dissolved O₂ and dissolved inorganic carbon in the Big Hole River, Montana, *Environ. Sci. Technol.*, 39, 7134–7140, 2005.
- Rantakari, M. and Kortelainen, P.: Controls of total organic and inorganic carbon in randomly selected Boreal lakes in varied catchments, *Biogeochemistry*, 91, 151–162, 2008.
- Raymond, P. A., Zappa, C. J., Butman, D., Bott, T. L., Potter, C., Mulholland, P., Laursen, A. E., McDowell, W. H., and Newbold, D.: Scaling the gas transfer velocity and hydraulic geometry in streams and small rivers, *Limnol. Oceanogr.*, 2, 41–53, doi:10.1215/21573689-1597669, 2012.
- Raymond, P. A., Hartmann, J., Lauerwald, R., Sobek, S., McDonald, C., Hoover, M., Butman, D., Striegl, R., Mayorga, E., Humborg, C., Kortelainen, P., Dürr, H., Meybeck, M., Ciais, P., and Guth, P.: Global carbon dioxide emissions from inland waters, *Nature*, 503, 355–359, doi:10.1038/nature12760, 2013.
- Richardson, D. C., Newbold, J. D., Aufdenkampe, A. K., Taylor, P. G., and Kaplan, L. A.: Measuring heterotrophic respiration rates of suspended particulate organic carbon from stream ecosystems, *Limnol. Oceanogr.-Meth.*, 11, 247–261, 2013.
- Richey, J. E., Devol, A. H., Wofsy, S. C., Victoria, R., and Riberio, M. N. G.: Biogenic gases and the oxidation and reduction of carbon in Amazon River and floodplain waters, *Limnol. Oceanogr.*, 33, 551–561, 1988.
- Richey, J. E., Melack, J. M., Aufdenkampe, A. K., Ballester, V. M., and Hess, L.: Outgassing from Amazonian rivers and wetlands as a large tropical source of atmospheric CO₂, *Nature*, 416, 617–620, 2002.
- SADC, SARDC, GRID-Arendal, and ZAMCOM: *Zambezi River Basin Atlas of the Changing Environment*, Southern African Development Community (SADC), Southern African Research and Documentation Centre (SARDC), United Nations Environment Programme (UNEP)/GRID-Arendal, Zambezi Watercourse Commission (ZAMCOM), Gaborone, Harare and Arendal, 134 pp., 2012.
- Sawakuchi, H. O., Bastviken, D., Sawakuchi, A. O., Krusche, A. V., Ballester, M. V. R., and Richey, J. E.: Methane emissions from Amazonian Rivers and their contribution to the global methane budget, *Glob. Change Biol.*, 20, 2829–2840, doi:10.1111/gcb.12646, 2014.
- Schlünz, B. and Schneider, R. R.: Transport of organic carbon to the oceans by rivers: reestimating flux and burial rates, *Int. J. Earth Sci.*, 88, 599–606, 2000.
- Tamoo, F., Van den Meersche, K., Meysman, F., Marwick, T. R., Borges, A. V., Merckx, R., Dehairs, F., Schmidt, S., Nyunja, J., and Bouillon, S.: Distribution and origin of suspended matter and organic carbon pools in the Tana River Basin, Kenya, *Biogeosciences*, 9, 2905–2920, doi:10.5194/bg-9-2905-2012, 2012.
- Tamoo, F., Borges, A. V., Meysman, F. J. R., Van Den Meersche, K., Dehairs, F., Merckx, R., and Bouillon, S.: Dynamics of dissolved inorganic carbon and aquatic metabolism in the Tana River basin, Kenya, *Biogeosciences*, 10, 6911–6928, doi:10.5194/bg-10-6911-2013, 2013.
- Teodoru, C. R., del Giorgio, P., Prairie, Y. T., and Camire, M.: pCO₂ dynamics in boreal streams of northern Quebec, Canada, *Global Biogeochem. Cy.*, 23, GB2012, doi:10.1029/2008GB003404, 2009.
- Teodoru, C. R., del Giorgio, P., and Prairie, Y. T.: Spatial heterogeneity of surface CO₂ fluxes in a newly created Eastmain-1 reservoir in northern Quebec, Canada, *Ecosystems*, 14, 28–46, doi:10.1007/s10021-010-9393-7, 2010.
- Tranvik, L. J., Downing, J. A., Cotner, J. B., Loiselle, S. A., Striegl, R. G., Ballatore, T. J., Dillon, P., Finlay, K., Knoll, L. B., Kortelainen, P. L., Kutser, T., Larsen, S., Laurion, I., Leech, D. M., McCallister, L. S., McKnight, D. M., Melack, J. M., Porter, J. A., Prairie, Y. T., Renwick, W. H., Roland, F., Sherman, B. S., Schindler, D. W., Sobek, S., Tremblay, A., Vanni, M. J., Verschoor, A. M., von Wachenfelds, E., and Weyhenmeyer, G. A.: Lakes and reservoirs as regulators of carbon cycling and climate, *Limnol. Oceanogr.*, 54, 2298–2314, doi:10.4319/lo.2009.54.6_part_2.2298, 2009.
- Waldron, S., Scott, E. M., and Soulsby, C.: Stable isotope analysis reveals lower-order river dissolved inorganic carbon pools are highly dynamic, *Environ. Sci. Technol.*, 41, 6156–6162, doi:10.1021/es0706089, 2007.
- Wang, Z. A., Bienvenu, D. J., Mann, P. J., Hoering, K. A., Poulsen, J. R., Spencer, R. G. M., and Holmes, R. M.: Inorganic carbon speciation and fluxes in the Congo River, *Geophys. Res. Lett.*, 40, 511–516, doi:10.1002/grl.50160, 2013.
- Weiss, F. R. and Price, B. A.: Nitrous oxide solubility in water and seawater, *Mar. Chem.*, 8, 347–359, 1980.
- Weiss, R. F.: Determinations of carbon dioxide and methane by dual catalyst flame ionization chromatography and nitrous oxide by electron capture chromatography, *J. Chromatogr. Sci.*, 19, 611–616, 1981.
- Wellington, J. H.: *Southern Africa – a Geographic Study*, vol. 1, Physical Geography, Cambridge University Press, Cambridge, 528 pp., 1955.
- Whitfield, P. H., Aherne, J., and Watmough, S.: Predicting the partial pressure of carbon dioxide in boreal lakes, *Can. Water Resour. J.*, 34, 415–426, 2009.
- World Bank.: *The Zambezi River Basin, A multi-sector investment opportunities analysis*, vol. 3: State of the basin, published by the International Bank for Reconstruction and Development/The World Bank, 1818 H Street NW, Washington DC 20433, USA, 202 pp., 2010.

- Worrall, F., Burt, T., and Adamson, J.: Fluxes of dissolved carbon dioxide and inorganic carbon from an upland peat catchment: implications for soil respiration, *Biogeochemistry*, 73, 515–539, doi:10.1007/s10533-004-1717-2, 2005.
- Yamamoto, S., Alcauskas, J. B., and Crozier, T. E.: Solubility of methane in distilled water and seawater, *J. Chem. Eng. Data*, 21, 78–80, 1976.
- Zurbrügg, R., Wamulume, J., Kamanga, R., Wehrli, B., and Senn, D. B.: River-floodplain exchange and its effects on the fluvial oxygen regime in a large tropical river system (Kafue Flats, Zambia), *J. Geophys. Res.*, 117, G03008, doi:10.1029/2011JG001853, 2012.